Non-Hermitian localization in biological networks

Ariel Amir,[1] Naomichi Hatano,[2] and David R. Nelson[1,3]

[1]*School of Engineering and Applied Sciences, Harvard University, Cambridge, Massachusetts 02138, USA*
[2]*Institute of Industrial Science, University of Tokyo, Komaba, Meguro, Tokyo 153-8505, Japan*
[3]*Department of Physics, Harvard University, Cambridge, Massachusetts 02138, USA*

We explore the spectra and localization properties of the N-site banded one-dimensional non-Hermitian random matrices that arise naturally in sparse neural networks. Approximately equal numbers of random excitatory and inhibitory connections lead to spatially localized eigenfunctions and an intricate eigenvalue spectrum in the complex plane that controls the spontaneous activity and induced response. A finite fraction of the eigenvalues condense onto the real or imaginary axes. For large N, the spectrum has remarkable symmetries not only with respect to reflections across the real and imaginary axes but also with respect to 90° rotations, with an unusual anisotropic divergence in the localization length near the origin. When chains with periodic boundary conditions become directed, with a systematic directional bias superimposed on the randomness, a hole centered on the origin opens up in the density-of-states in the complex plane. All states are extended on the rim of this hole, while the localized eigenvalues outside the hole are unchanged. The bias-dependent shape of this hole tracks the bias-independent contours of constant localization length. We treat the large-N limit by a combination of direct numerical diagonalization and using transfer matrices, an approach that allows us to exploit an electrostatic analogy connecting the "charges" embodied in the eigenvalue distribution with the contours of constant localization length. We show that similar results are obtained for more realistic neural networks that obey "Dale's law" (each site is purely excitatory or inhibitory) and conclude with perturbation theory results that describe the limit of large directional bias, when all states are extended. Related problems arise in random ecological networks and in chains of artificial cells with randomly coupled gene expression patterns.

I. INTRODUCTION

The simplest models of neural networks assume long-range connectivity between individual neurons in the brain, leading to synaptic matrices $M(i,j)$ with connection strengths approximately independent of the separation $r_{ij} = |\vec{r}_i - \vec{r}_j|$ in three dimensions. The eigenvalue spectrum of $M(i,j)$ controls the spontaneous activity and induced response of the network, and much is known when its elements are chosen from simple random matrix ensembles in the limit of large matrix rank N. For example, classic treatments of the spectra of real symmetric random matrices leading to the Wigner semicircular density-of-states describing the distribution of real eigenvalues [1,2] have been generalized by Sommers *et al.* [3] to allow for a tunable asymmetry in Gaussian probability distributions for the matrix elements $M(i,j)$ and $M(j,i)$. These authors introduce a parameter that interpolates between the Hermitian limit ($M(i,j) = M(j,i)$) studied by Wigner [4] and the case of fully asymmetric matrices where $M(i,j)$ and $M(j,i)$ are independent random variables. In the latter, non-Hermitian limit, the semicircular eigenvalue distribution on the real axis is replaced by the 'circular law' [5,6], where the eigenvalues are now uniformly distributed inside a circle in the complex plane, with a vanishing fraction lying outside the circle in the limit $N \to \infty$. For the general case, Sommers *et al.* found that the eigenvalue distribution is uniform inside an *ellipse*, whose aspect ratio along the real and imaginary axes varies with the amount of non-Hermiticity [3].

As pointed out by Rajan and Abbott [7], typical applications to neuroscience require that each node in a synaptic conductivity network be either purely excitatory or inhibitory (Dale's law), which leads to constraints on the signs of the matrix elements $M(i,j)$: All entries in a row describing an excitatory neuron must be positive or zero, and all entries in an inhibitory row must be negative or zero. These authors then studied eigenvalue spectra of random matrices with long-range connectivity, with excitatory and inhibitory networks drawn from distributions with different means and with equal or different standard deviations. When the strengths of the excitatory and inhibitory connections are appropriately balanced, with equal standard deviations, the eigenvalue distributions can be made to obey the circular law by imposing a mild constraint. However, when the standard deviations differ, the eigenvalue density becomes nonuniform within a circle in the complex plane.

Less is known for N-site *banded* random matrices with signed matrix elements, which might be an approximate model for neural networks such that $M(i,j) \sim \exp[-|\vec{r}_i - \vec{r}_j|/l]$, where l^d (in d dimensions) is often a large volume containing as many as 10^5 neurons. On spatial scales larger than l, the synaptic connectivity matrix becomes sparse, with the largest elements concentrated along the diagonal. Banded Hermitian random matrices in d dimensions, frequently studied in the context of solid-state physics, have long been known to have eigenvalue spectra characterized by a large number of spatially *localized* eigenfunctions [8,9], and it is this phenomenon that we wish to study here. To focus on an extreme example of bandedness, consider a matrix describing a one-dimensional chain of N sites, where only the elements $M(j,j)$, $M(j,j+1)$ and $M(j+1,j)$ describing on-site and nearest-neighbor couplings can be nonzero. If we wish to impose periodic boundary conditions, then we will set $M(i,j) = M(i,j+N) = M(i+N,j), \forall i,j$. If the lattice spacing $a \approx l$, then this model is a rough approximation to the denser neural networks discussed above, coarse grained out

to a scale of order l, with each site representing the spatially averaged firing rates of many actual neurons. We concentrate here on off-diagonal randomness, and assume that all $\boldsymbol{M}(j,j)$ are identical, and describe, say, a site-independent damping to a background firing rate. For the Hermitian case, with $\boldsymbol{M}(j,j+1) = \boldsymbol{M}(j+1,j)$ chosen from some probability distribution, nearly all states are localized in the limit of large N, with the longest localization lengths occurring near the band center and the shortest localization lengths near the band edges [9]. See Appendix A for a brief review and numerical illustration of this solid-state physics example, which provides a useful benchmark for the more intricate problem with complex eigenvalues we study here. Chaudhari *et al.* [10] have studied a related problem, with Hermitian coupling strengths falling off exponentially in space and random self-couplings (diagonal randomness), in the context of one-dimensional neural networks, as well as localization of the eigenmodes in a non-Hermitian matrix arising not from disorder but from a slow gradient in the diagonal elements. Here we study sparse *non-Hermitian* matrices and the localization properties of their eigenmodes. An important feature of our model is the underlying *spatial* structure (the connections are between nearest neighbors in real space), which distinguishes our work from recent, interesting studies of sparse non-Hermitian matrices without such structure [11–13].

A. From neural networks to random matrices

As stated above, we focus here on *off-diagonal* randomness in the neural connections, which is both non-Hermitian [$\boldsymbol{M}(j,j+1) \neq \boldsymbol{M}(j+1,j)$] and, importantly, also allows for $\boldsymbol{M}(j,j+1)$ and $\boldsymbol{M}(j+1,j)$ to be of *opposite sign* roughly 50% of the time. We thus model a set of approximately balanced excitatory and inhibitory nearest-neighbor neural connections in one dimension and study the localization properties of the intricate complex eigenvalue spectrum that results. To put our investigations in context, consider first (using a convenient Dirac notation $|j\rangle$ to describe a neuron at site j) the spectrum of a simple *Hermitian* one-dimensional (1D) tridiagonal matrix with random connections, namely

$$\boldsymbol{M} = -\sum_{j=1}^{N} [s_j^+ |j\rangle\langle j+1| + s_j^- |j+1\rangle\langle j|],$$
$$s_j^+ = s_j^- = s_0 + s_j > 0, \tag{1}$$
$$s_j \in [-\Delta, \Delta], \quad \Delta = 0.5 s_0.$$

Here all eigenvalues are real, and the symmetrical connections $s_j^+ = s_j^-$ between neighboring sites are guaranteed to be positive by our choice of a relatively narrow ($\Delta < s_0$) box distribution for the bond-to-bond fluctuations in the connection strengths relative to the background level s_0, and we have subtracted off a diagonal contribution, assumed to be site-independent. As shown in Appendix A, the localization length $\xi(\varepsilon)$ of the eigenfunctions diverges near the band center at energy $\varepsilon = 0$. The quantity $\xi(\varepsilon)$ describes the spatial scale over which an eigenfunction with energy ε is nonzero. If the eigenfunction $\phi_\varepsilon(j)$ is large near a "center of localization" j^*, then, roughly speaking, its envelope decays like $\exp[-|j-j^*|/\xi(\varepsilon)]$. The localization length $\xi(\varepsilon)$ is known to diverge logarithmically [14], $\xi(\varepsilon) \sim \log(1/\varepsilon^2)$, as
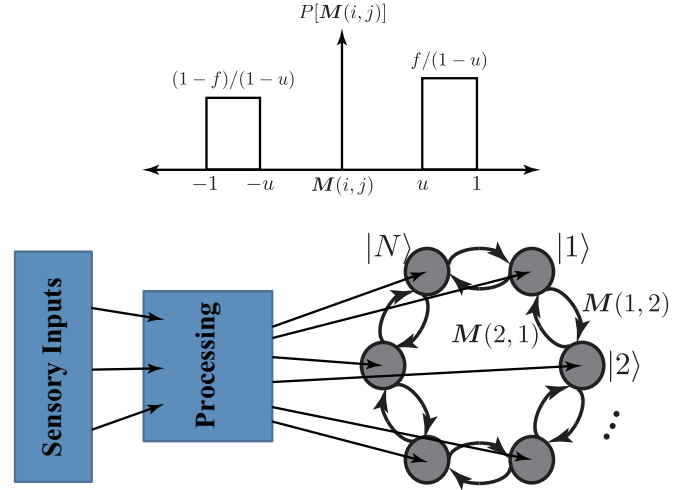

FIG. 1. Schematic of a 1D neural network problem with periodic boundary conditions. Sensory inputs, possibly after a processing step, are sent via feed-forward couplings into a circular ring of N neurons $|j\rangle, j = 1, \ldots, N$, with nearest-neighbor excitatory and inhibitory connections. $\boldsymbol{M}(1,2)$ and $\boldsymbol{M}(2,1)$ can be not only unequal but also of opposite sign if one direction is excitatory and the other inhibitory. Inset shows the probability distribution of a generic nearest-neighbor coupling strength s.

$\varepsilon \to 0$. As discussed in Appendix A, for one-dimensional Hermitian localization problems there is an elegant relation connecting the density-of-states $\rho(\varepsilon)$ to the localization length $\xi(\varepsilon)$, known as the Thouless relation [15]. In this case, the Thouless relation implies a strongly diverging density-of-states, $\rho(\varepsilon) \sim 1/[|\varepsilon| \log^3(1/\varepsilon^2)]$, near the origin. We shall see echoes of these results later in this paper.

We study here a generalization of Eq. (1) that arises in one-dimensional neural networks with random excitatory and inhibitory nearest-neighbor connections. Following Chapter 7 of Ref. [16], consider the sparse "recurrent neural network" shown in Fig. 1, a chain of nodes with asymmetric connections between nearest neighbors and with periodic boundary conditions. Sensory inputs, possibly after a processing step, are sent via feed-forward couplings into a circular ring of N neurons $|j\rangle, j = 1, \ldots, N$. The nearest-neighbor excitatory and inhibitory couplings $\boldsymbol{M}(j,j+1)$ and $\boldsymbol{M}(j+1,j)$ can be not only unequal but also of opposite sign if one direction is excitatory and the other inhibitory. Consider a model where the average firing rates v_i and v_j in neurons i and j (a coarse-grained description of the temporal density of discrete spikes in these neurons) are coupled together and obey

$$\tau \frac{dv_i}{dt} = -v_i + F(\boldsymbol{M}_{ij} v_j + h_i). \tag{2}$$

Here $\boldsymbol{M}_{ij} \equiv \boldsymbol{M}(i,j)$, τ is a characteristic neuron time constant (assumed for simplicity to be the same for all neurons), and we use the summation convention. Inputs to an animal brain from the outside, due to whiskers, retinal cells, olfaction, etc. (after a possible processing step), are represented by $h_i = \boldsymbol{W}_{ij} u_j$, where the connection matrix $\boldsymbol{W}_{ij} \equiv \boldsymbol{W}(i,j)$ and the input firing rates $\{u_i\}$ represent the feed-forward part of this network. The activation function $F(w)$ (often taken to have a nonlinear sigmoidal shape [16,17]) insures that the

firing rates are bounded above (when inhibitory connections are present, additional constraints can be imposed to ensure that the firing rates can never be negative [16]). Here we assume for simplicity that the activation function is the same for both excitatory and inhibitory connections. The eigenvalues and eigenvectors of the matrix $\boldsymbol{M}_{ij}$ are clearly important for understanding the behavior of a linearized version of Eq. (2),

$$\tau \frac{dv_i}{dt} = -v_i + \boldsymbol{M}_{ij} v_j + h_i, \tag{3}$$

where we assume without loss of generality that $F(0) = 0$ and $F'(0) = 1$. This linear recurrent network is capable of both selective amplification and input integration [16]. More generally, knowledge of the eigenvalues and eigenfunctions of $\boldsymbol{M}_{ij}$ is useful for studying spontaneous activity and evoked responses [18,19]. Spontaneous activity depends on whether the real parts of any of the eigenvalues are large enough to destabilize the silent state in a linear analysis, and the spectrum of eigenvalues with large real parts provides valuable information about the spontaneous activity in the full, nonlinear models and about the localization volume determining the size of the active clusters carrying out computations. Moreover, similar matrices arise when nonlinear problems are linearized about a steady state.

To see why *random* neural connections might be relevant, note that these can be formed during development, with many random attachments of axons and dendrites to other neurons. Then, over time, pruning (loss of connections) and adaptation (strengthening and weakening of various excitatory and inhibitory connections) occur as neural circuits "learn" various functions. The likely result is a mixture of structured and random components. The spectra and eigenfunctions of completely random sparse neural network chains, with a mixture of inhibitory and excitatory connections, could provide a description of neural activity during the early stages of development and is also a useful reference model. Similar justifications have been advanced for studying the dense neural networks that obey Dale's law treated in Ref. [7].

B. Model and density-of-states

With this motivation, we now discuss the spectra of non-Hermitian matrices that generalize Eq. (1), namely

$$\boldsymbol{M} = \sum_{j=1}^{N} [s_j^+ e^g |j+1\rangle\langle j| + s_j^- e^{-g} |j\rangle\langle j+1|], \tag{4}$$

where for most of this paper we impose periodic boundary connections, $|j+N\rangle = |j\rangle$. The constant diagonal contribution associated with Eq. (3) has again been subtracted off. The connection strengths s_j^+ and s_j^- are independent and identically distributed random variables chosen from a probability distribution $P(s_j^\pm)$, given by (see inset to Fig. 1),

$$P(s) = \begin{cases} \frac{f}{1-u} & \text{for} \quad u < s < 1, \\ \frac{1-f}{1-u} & \text{for} \quad -1 < s < -u, \\ 0, & \text{otherwise.} \end{cases} \tag{5}$$

The parameter u, $0 < u \leqslant 1$, controls the width of the positive and negative parts of the distribution, while f, $0 < f < 1$, determines the ratio of inhibitory to excitatory connections.

This functional form excludes connections that are very close to zero, which would bias the 1D network towards falling apart into disjoint pieces. The coupling g in Eq. (4) controls the strength of a systematic clockwise ($g > 0$) or counterclockwise ($g < 0$) bias in the strengths of positive and negative neural connections around the ring. As we shall see, nonzero g can have a remarkable effect on the spectrum and localization properties. In this paper, we concentrate on the spectra and localization properties of eigenfunctions in the approximately balanced case, $f \approx 1/2$, which represents the greatest departure from conventional Hermitian localization problems in one dimension [8–10,14,15]. For now, we suppress the neuroscience constraints associated with Dale's law, as might be appropriate if each node in the chain describes a large number of strongly coupled neurons randomly chosen to be excitatory and inhibitory. However, we shall later argue (Sec. II C) that a straightforward modification of Eq. (4) that respects Dale's law produces negligible changes in the spectra and localization properties in the limit of large N.

The case of $f = 1$ with $0 < u < 1$ (random excitatory connections only) is related to earlier work on the random non-Hermitian 1D matrices that arise from the physics of randomly pinned superconducting vortex lines [20,21] and in the population dynamics of heterogeneous 1D environments [22,23]. When $g > 0$, this problem is sometimes referred to as "directed localization" [24,25], terminology we adopt here as well. The spectrum of models with $f = 1/2$ and $u = 1$ (i.e., $\boldsymbol{M}(j, j+1) = \pm 1$ and $\boldsymbol{M}(j+1, j) = \pm 1$, excitatory and inhibitory connections chosen at random with equal probabilities) has also been studied before [26–32] and has been shown to have an extremely rich structure. Here we explore the *localization* properties of the eigenfunctions associated with these spectra for a range of u values in some detail.

Figures 2(a) and 2(b) exhibit the remarkable spectra associated with Eqs. (4) and (5) when $f = 1/2$, $u = 1$ and for $g = 0$ and $g = 0.1$, respectively. To the best of our knowledge, the striking spectrum in Fig. 2(a) first appeared in a 1999 paper by Feinberg and Zee [26], who mentioned that this model might have interesting localization properties. Although the eigenvalues are in general complex, when $g = 0$, a significant fraction of them (about 20%) have condensed onto the real axis, see Fig. 3; similarly, about 20% have condensed onto the imaginary axis. In Appendix B this numerical analysis is extended to the case of $u \neq 1$, with similar results. For large N, the density-of-states is symmetric under reflections across the real and imaginary axes, as well as across $\pm 45°$ lines in the complex plane, as we shall show in Sec. II. The remaining eigenvalues (approximately 60%) form an intricate, diamond-shaped structure. When u is near 1, the density-of-states appears to acquire a fractal-like boundary. See Appendix B for a summary of the density-of-states for the more general probability distribution of Eq. (5) for arbitrary u and $f = 1/2$.

C. Main results

We are now in a position to summarize our main results. In Sec. II we discuss various symmetries associated with the density-of-states of the models studied here. In Sec. III we show that almost all eigenfunctions are localized (similar to
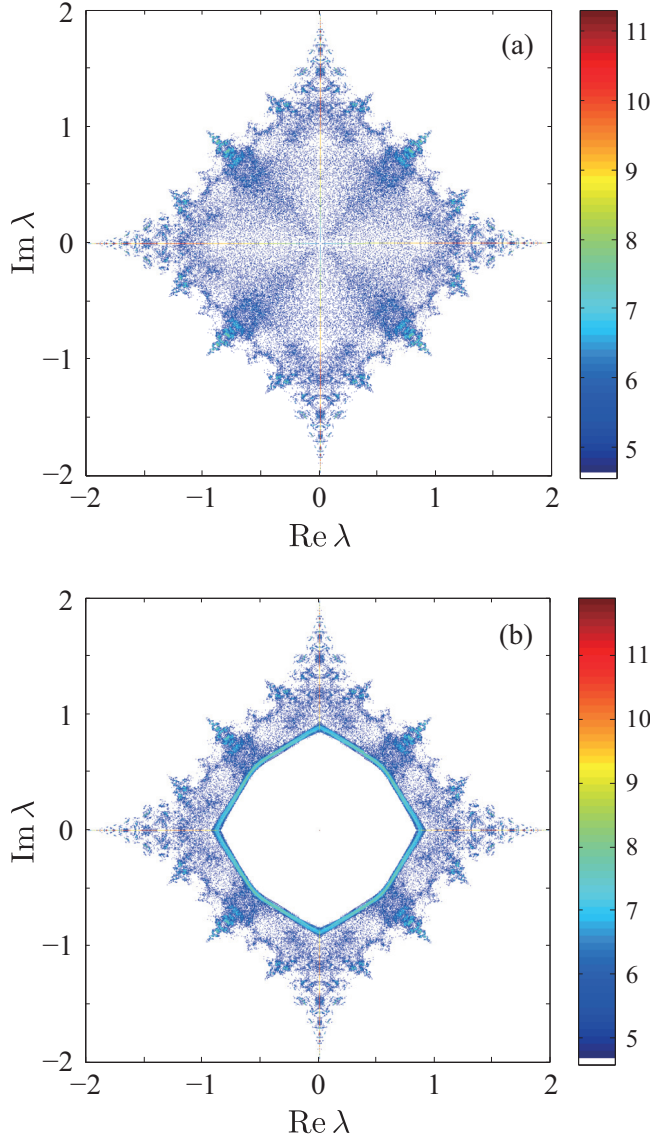
FIG. 2. (a) Density-of-states (DOS) of the complex eigenvalue spectrum for the sparse random matrix defined by $f = \frac{1}{2}$ and $u = 1$ with $g = 0$ obtained through exact diagonalization of 10 000 matrices of dimension 5000×5000. The scale is logarithmic, and the white background denotes areas where the DOS vanishing. The only randomness is in the signs of the connections, $\boldsymbol{M}(j, j + 1) = \pm 1$, $\boldsymbol{M}(j + 1, j) = \pm 1$. (b) Density-of-states for the case $g = 0.1$; all other parameters are identical to (a).

FIG. 3. DOS on the real axis for the parameters of Fig. 2(a), comprising close to 20% of all eigenvalues.

the 1D Hermitian case of Appendix A), with the smallest localization lengths near the boundary of the spectrum in the complex plane and a diverging localization length near the origin. Our analysis of localization in this model has been guided by the work of Derrida *et al.* [33] on a related problem (with unimodular *complex* random couplings between sites), who derive an elegant generalization of the Thouless formula for eigenvalues in the complex plane: The inverse localization length is the two-dimensional electrostatic potential associated with a collection of charges at the eigenvalue locations in the complex plane. Our numerical analysis strongly suggests that the localization length diverges as the modulus of the
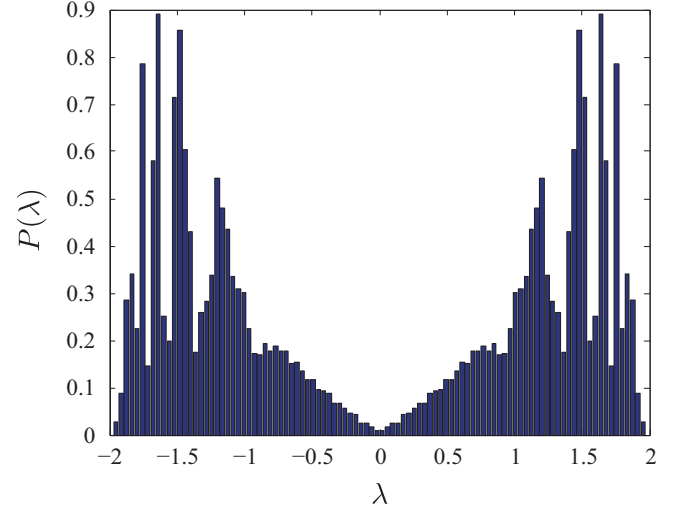
eigenvalues tends to zero. Indeed, if the eigenvalues are written $\lambda = \lambda_1 + i\lambda_2$, where λ_1 and λ_2 are real, a numerical study of the inverse localization length defined via the product of N random 2×2 transfer matrices [34–36] for u near 1 leads to the following ansatz:

$$\xi(\lambda_1, \lambda_2) \propto \frac{1}{(|\lambda_1| + |\lambda_2|)\sqrt{\lambda_1^2 + \lambda_2^2}}, \qquad (6)$$

which should be compared to the much weaker logarithmic divergence discussed in Appendix A for 1D Hermitian hopping randomness. Although the divergence shown in Eq. (6) only holds for u near 1, the infinite localization length at the origin is more general, as discussed in Sec. III E.

As shown in Fig. 2(b), a hole surrounding the origin with angular corners opens up in the complex plane when these calculations are repeated for a clockwise bias parameter $g = 0.1$. A similar hole opens up in the Feinberg-Zee model of Ref. [26], with complex unimodular hopping matrix elements [37]. As we demonstrate in Sec. III, a large number of *extended* states now occupies the rim of hole. For large N, the eigenvalues of the localized states outside the hole are unchanged, a spectral rigidity property that can be derived from a simple exponential "gauge transformation" acting on the corresponding eigenfunctions for $g = 0$, see Ref. [20]. A corollary is that the g-dependent shape of holes like that in Fig. 2(b) tracks the $g = 0$ contours of constant localization length, with a diverging localization length as the rim is approached from the outside.

What happens to directed localization for neural networks that obey Dale's law, as studied for spatially extended neural connections in Ref. [7]? In Sec. II C, we argue that the above results should be unchanged for large N. We will do this by replacing the matrix $\boldsymbol{M}$ with a modified connectivity matrix,

$$\boldsymbol{G} = \sum_{k=1}^{N} \sigma_k [e^g |k+1\rangle\langle k| + e^{-g} |k-1\rangle\langle k|], \qquad (7)$$

$$|k+N\rangle = |k\rangle,$$

where the N real random numbers $\{\sigma_k\}$ are chosen from the probability distribution $P(\sigma_k)$, again given by Eq. (5). Figure 7 illustrates a particular example of the Dale's law connectivity matrix for $N = 5$. Note that the nonzero connections in the same row have the same sign. Equation (7) has site randomness, as opposed to the bond randomness displayed in Eq. (4). Despite the fact that $2N$ random numbers are necessary to specify $\boldsymbol{M}$ and only N random numbers specify $\boldsymbol{G}$, we show via similarity transformations in Sec. II C that the spectra and localization properties of $\boldsymbol{M}$ and $\boldsymbol{G}$ are essentially identical, a result which we have also confirmed numerically. The underlying reason is that the spectral properties are determined in both cases by above- and below-diagonal products such as $\boldsymbol{M}(j, j+1) \cdot \boldsymbol{M}(j+1, j) = s_j^+ s_j^-$ and $\boldsymbol{G}(j, j+1) \cdot \boldsymbol{G}(j+1, j) = \sigma_j \sigma_{j+1}$. These quantities have identical statistical properties.

In Sec. IV we discuss large-g perturbation theory, which focuses on the changes in the eigenvalues and eigenfunctions which are all extended in this limit. This analysis can be carried out for arbitrary f and u, although it cannot capture the localization that results as the eigenvalues move toward the origin with decreasing g.

We note that some of our results rely on the underlying symmetries inherent in our model, which can be divided into two bipartite sublattices, with the matrix M having nonvanishing elements only between different sublattices. Diagonal disorder, for example, will break this assumption and would be present in more realistic descriptions of networks. For this reason, some of the results presented are not expected to be robust, in particular, the divergence of the localization length at the origin (Sec. III E) and the symmetry between real and imaginary axis (Sec. II). However, the delocalization transition occurring as one adds a bias to the network, and the hole arising in the DOS as a result of it, appear to be robust features that are largely independent of the details and are the key results of our work.

Section V contains a summary and outlook, as well as a brief discussion of related models, including diagonal randomness and neural clusters coupled to form a ring. Appendices A–C describe, respectively, a Hermitian random hopping model, the density-of-states for arbitrary u, and second-order perturbation theory for large g.

II. SYMMETRIES ASSOCIATED WITH THE DENSITY-OF-STATES

In order to discuss spectral symmetries, we first introduce a similarity transformation that is applicable to the present model with open boundary conditions. Consider an $N \times N$ tridiagonal matrix of the form

$$
\boldsymbol{A} = \begin{pmatrix} d_1 & b_1 & & & & 0 \\ a_1 & d_2 & b_2 & & & \\ & a_2 & d_3 & b_3 & & \\ & & \ddots & \ddots & \ddots & \\ & & & a_{N-2} & d_{N-1} & b_{N-1} \\ 0 & & & & a_{N-1} & d_N \end{pmatrix}, \quad (8)
$$

where $\{a_x\}$, $\{b_x\}$, and $\{d_x\}$ are arbitrary real numbers and all other entries vanish. We can symmetrize this matrix by a diagonal similarity transformation, whose jth matrix element reads

$$
\boldsymbol{S}_{jj} = \prod_{k=1}^{j-1} \sqrt{\frac{a_k}{b_k}}, \quad (9)
$$

which we may call a generalized gauge transformation [20]. The result of this symmetrization reads

$$
\boldsymbol{A}' = \boldsymbol{S}^{-1} \boldsymbol{A} \boldsymbol{S} = \begin{pmatrix} d_1 & c_1 & & & & 0 \\ c_1 & d_2 & c_2 & & & \\ & c_2 & d_3 & c_3 & & \\ & & \ddots & \ddots & \ddots & \\ & & & c_{N-2} & d_{N-1} & c_{N-1} \\ 0 & & & & c_{N-1} & d_N \end{pmatrix},
$$

$$(10)$$

where

$$
c_j = \sqrt{a_j b_j}. \quad (11)
$$

The matrices (8) and (10) are isospectral, due to the properties of similarity transformations.

Note that the spectrum of the matrix $\boldsymbol{A}'$ depends only on the product of the opposing off-diagonal elements a_j and b_j and not independently on each of them (as also follows from calculating the characteristic polynomial of the matrix $\boldsymbol{A}$). Another important observation is that the matrix (10) is real and symmetric if a_j and b_j have the same sign but is non-Hermitian otherwise. The non-Hermitian Anderson chains proposed in Refs. [38] and [20], in which all a_j and b_j are negative, therefore would have only real eigenvalues unless we introduced periodic boundary conditions. If the matrix (8) has nonzero corner elements a_N for $\boldsymbol{A}_{1N}$ and b_N for $\boldsymbol{A}_{N1}$ (thus coupling the chain into a ring), then the resulting matrix $\boldsymbol{A}' = \boldsymbol{S}^{-1} \boldsymbol{A} \boldsymbol{S}$ has nonzero corner matrix elements

$$
\boldsymbol{A}'_{1N} = (\boldsymbol{S}^{-1} \boldsymbol{A} \boldsymbol{S})_{1N} = \sqrt{a_N b_N} \prod_{j=1}^{N} \sqrt{\frac{a_j}{b_j}}, \quad (12)
$$

$$
\boldsymbol{A}'_{N1} = (\boldsymbol{S}^{-1} \boldsymbol{A} \boldsymbol{S})_{N1} = \sqrt{a_N b_N} \prod_{j=1}^{N} \sqrt{\frac{b_j}{a_j}}, \quad (13)
$$

which make the matrix non-Hermitian and allow the possibility of complex eigenvalues unless

$$
\prod_{j=1}^{N} a_j = \prod_{j=1}^{N} b_j. \quad (14)
$$

Although this similarity transformation leaves the diagonal randomness intact, it packs all effects of the random, non-Hermitian hopping terms into a single pair of corner matrix elements. This perspective is useful already for simple cases where the elements $\{a_j\}$ and $\{b_j\}$ in Eq. (8) can differ but are both constrained to be of the same sign. Let us take $a_j = e^{-g} s_j^- > 0$ and $b_j = e^g s_j^+ > 0$, consistent with Eq. (4), so the corner matrix element $\boldsymbol{A}'_{N1}$ takes the form

$$
\boldsymbol{A}'_{N1} = \sqrt{s_N^- s_N^+} \, e^{Ng} \prod_{j=1}^{N} \sqrt{\frac{s_j^+}{s_j^-}}. \quad (15)
$$

If we now choose the elements $\{s_j^{\pm}\}$ according to the probability distribution of Eq. (5) with $f = 1$ and $0 < u < 1$, then all $s_j^{\pm}$ will be positive, and A'_{N1} is real and described by a log-normal distribution. It is simpler to study $\log A'_{N1}$, which behaves like a random walk. As discussed in Sec. III, a closely related quantity determines the localization properties of eigenfunctions as function of g. Focusing for simplicity on the case $u = 0^+$, we readily find

$$\langle \log A'_{N1} \rangle = Ng - 1 \qquad (16)$$

and

$$\langle (\log A'_{N1} - \langle \log A'_{N1} \rangle)^2 \rangle = \frac{N}{4} + O(1/N), \qquad (17)$$

where $\langle \bullet \rangle$ represents an average over the disorder and similar results obtain for $0 < u < 1$. Upon defining an effective directional bias parameter $g_{\text{eff}} \equiv \langle \log A'_{N1} \rangle / N$, we see that if microscopic bias is $g = 0$, then the hopping randomness represented by the elements $\{s_j^{\pm}\}$ leads to a $g_{\text{eff}} = O(1/N^{1/2})$, which vanishes in the limit large N. Thus, the hopping disorder is effectively undirected as $N \to \infty$ in this case. When diagonal randomness is also present, we expect that the localized states will remain localized with real eigenvalues, unless g exceeds a critical value g_{c1} given by the minimum inverse localization length when $g = 0$.

If a_j and b_j can have different signs, then the matrix (8) is inherently non-Hermitian and can have complex eigenvalues with or without periodic boundary terms. It is this interesting case we focus on in the present paper. As discussed below, coupling the chain into a ring is crucial when $g > 0$.

A. Spectrum of sign-random model

Let us apply the above considerations to the sign-random non-Hermitian tight-binding chain given by the $N \times N$ matrix corresponding to Eq. (4) with $g = 0$:

$$\boldsymbol{M} = \begin{pmatrix} & s_1^+ & & & & & \\ s_1^- & & s_2^+ & & & & \\ & s_2^- & & s_3^+ & & & \\ & & s_3^- & & \ddots & & \\ & & & \ddots & & \ddots & \\ & & & & \ddots & & s_{N-1}^+ \\ & & & & & s_{N-1}^- & \end{pmatrix}, \qquad (18)$$

where all remaining elements, including diagonal ones, vanish, and each of $s_j^{\pm}$ are randomly set to be ± 1 with probability $1/2$. Spectra found by numerical diagonalization of a random sample are shown in Fig. 4 for $N = 10$, 1000, and 10 000, which should be compared with the disorder-averaged spectrum shown in Fig. 2(b). As discussed below, when $g = 0$ we can neglect the corner matrix elements.

We can describe the symmetries of the spectrum in the following way: First, since the matrix (18) is real, namely, $\boldsymbol{M} = \boldsymbol{M}^*$, if there is an eigenvalue λ_n, then there must be another eigenvalue λ_n^*. In other words, the spectrum is symmetric with respect to reflections across the real axis. Second, we consider flipping all signs of the hopping elements, transforming $\boldsymbol{M}$ to $-\boldsymbol{M}$, which is achieved by a chiral transformation of flipping

FIG. 4. The spectra on complex planes of the matrix (18) for (a) $N = 100$, (b) $N = 1000$, and (c) $N = 10\,000$.

signs of the bases every other site. Since the spectrum depends only on the product of s_x^+ and s_x^-, this transformation does not change the spectrum, proving the chiral symmetry of the matrix $\boldsymbol{M}$. In other words, if there is an eigenvalue λ_n, there must be another eigenvalue $-\lambda_n$, and hence the spectrum is symmetric under inversion in the complex plane $\lambda \to -\lambda$.
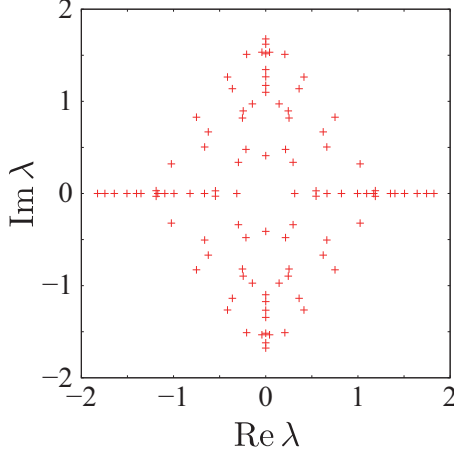
FIG. 5. The spectrum on a complex plane of the matrix (18), this time *with* additional boundary elements; compare it with Fig. 4(a). The system size is $N = 100$.

Finally, we argue that the spectrum has statistical symmetry with respect to the reflections across the $45°$ lines $\mathrm{Re}\, E = \pm\,\mathrm{Im}\, E$. According to the argument in the beginning of this section, the spectrum depends only on whether the product $s_x^+ s_x^-$ is $+1$ or -1. In other words, the randomness of the matrix (18) is caused by independent probability distributions of $N - 1$ independent degrees of freedom, $\{s_x^+ s_x^-\}$, instead of $2N - 1$. Let us then consider the spectrum of the matrix $i\boldsymbol{M}$. By multiplying every matrix element by $i = \sqrt{-1}$, we flip the sign of the product of the opposing off-diagonal elements which, however, does not change the binomial distribution of the $N - 1$ pieces of random variables when $f = 1/2$. Therefore, the matrices $\boldsymbol{M}$ and $i\boldsymbol{M}$ are statistically isospectral. Since the spectrum of $i\boldsymbol{M}$ is given by the $90°$ rotation of that of $\boldsymbol{M}$, the spectrum is statistically symmetric with respect to this operation. Combining this symmetry with the other symmetries, we conclude that it is statistically symmetric with respect to reflections around the $45°$ lines. The fact that the symmetry becomes better as we increase the system size underlines the observation that the symmetry is indeed statistical.

Adding the boundary elements $\boldsymbol{M}_{1N} = s_N^+$ and $\boldsymbol{M}_{N1} = s_N^-$ does not change the spectrum in an essential way when $g = 0$; their first-order perturbation to an eigenvalue λ_n with its normalized left and right eigenvectors $\langle\tilde{\psi}_n|$ and $|\psi_n\rangle$ (we use the tilde symbol to emphasize that they are not Hermitian conjugate to each other) is of order $1/N$ at most (and is exponentially small if the eigenfunctions are localized). Indeed, comparison of numerical results of Figs. 4(a) and 5 with and without the boundary elements suggests that they are not only statistically the same but also almost identical with occasional differences, even for $N = 100$.

B. Asymmetric amplitudes

Let us next introduce asymmetric amplitudes to the sign-random tight-binding model. Following Refs. [20,22,38], we express the asymmetry in the form [equivalent to Eq. (4)]

$$\boldsymbol{M}(g) = \begin{pmatrix} & e^g s_1^+ & & & e^{-g} s_N^- \\ e^{-g} s_1^- & & e^g s_2^+ & & \\ & e^{-g} s_2^- & & \ddots & \\ & & \ddots & & \ddots & \\ & & & \ddots & & \ddots \\ & & & & \ddots & & e^g s_{N-1}^+ \\ e^g s_N^+ & & & & e^{-g} s_{N-1}^- \end{pmatrix},$$

$$(19)$$

where we assume $g > 0$ without loss of generality. Note here that we have included the boundary terms $e^g s_N^+$ and $e^{-g} s_N^-$; if not, then the spectrum would be g independent because it would depend only on the product of the opposing off-diagonal elements. The diagonal similarity transformation

$$\boldsymbol{T}(g)_{xx} = e^{-g(x-1)} \tag{20}$$

changes the matrix $\boldsymbol{M}(g)$ into

$$\boldsymbol{M}'(g) = \boldsymbol{T}(g)^{-1}\boldsymbol{M}(g)\boldsymbol{T}(g)$$
$$= \begin{pmatrix} & s_1^+ & & & e^{-Ng} s_N^- \\ s_1^- & & s_2^+ & & \\ & s_2^- & & \ddots & \\ & & \ddots & & \ddots \\ & & & \ddots & & s_{N-1}^+ \\ e^{Ng} s_N^+ & & & & s_{N-1}^- \end{pmatrix}, \tag{21}$$

which shows that the boundary elements are essential in having a strong dependence on g.

As was discussed in Refs. [20,38], the spectrum of $\boldsymbol{M}(g)$ can in fact be an indicator of the localization of the eigenfunctions. Suppose that the eigenfunction ψ_n of an eigenvalue λ_n of the original Hamiltonian $\boldsymbol{M} = \boldsymbol{M}(0)$ is localized around a site x_0 and behaves approximately as

$$\psi_n(x) \sim e^{-\kappa_n|x-x_0|} \tag{22}$$

except for a phase factor. This quantity is also an approximate eigenfunction of $\boldsymbol{T}(g)^{-1}\boldsymbol{M}(g)\boldsymbol{T}(g)$, because the first-order perturbative corrections due to the boundary elements are exponentially small, of order $e^{-N(\kappa_n-g)}$, when $g < \kappa_n$. Thus, the corresponding eigenfunction of $\boldsymbol{M}(g)$ is given by

$$\psi_n(x; g) \sim e^{-gx-\kappa_n|x-x_0|}, \tag{23}$$

except for a phase factor. Indeed, the periodic boundary conditions are almost precisely satisfied for large N if $g < \kappa_n$; the discrepancy at the boundary is exponentially small, of order $e^{-N(\kappa_n-g)}$. Therefore, the eigenvalue λ_n of $\boldsymbol{M}(0)$ remains to be an eigenvalue of $\boldsymbol{M}(g)$ when $g < \kappa_n$. This argument breaks down when $g > \kappa_n$, for which the eigenvalue now moves as a function of g, with motion starting when $g = \kappa_n$. The numerical diagonalization of a random sample with $g = 0.1$ gives Fig. 6(a). According to the above argument (elaborated in Sec. III in detail), the states on the inner curve similar to an octagon have $\kappa = 0.1$ for $g = 0$, and vanishing κ for $g = 0.1$.
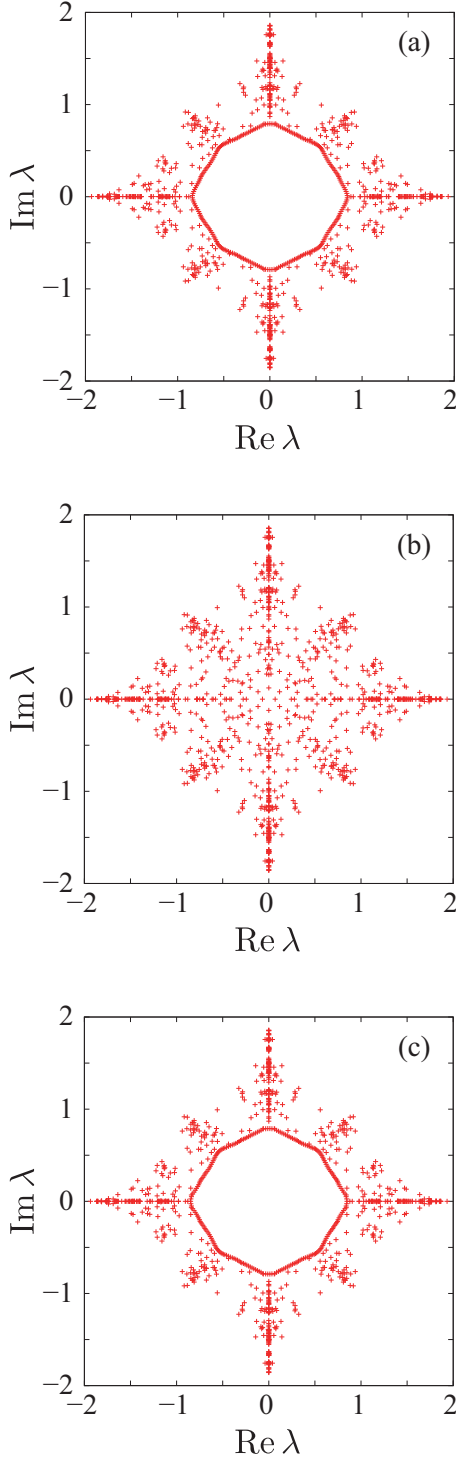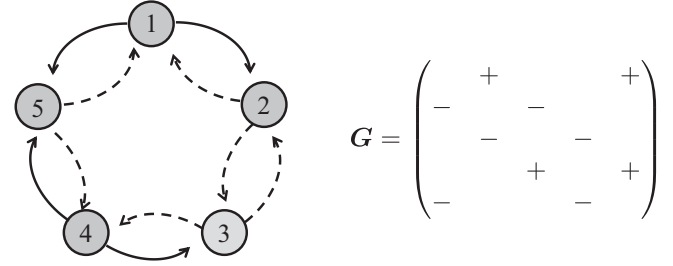
FIG. 7. Ring with $N = 5$ coupled neurons obeying Dale's law: each neuron couples in a purely excitatory or purely inhibitory manner to its two neighbors; solid arrows represent positive, excitatory connections, and dashed lines negative, inhibitory ones. The 5×5 matrix $\boldsymbol{G}$ corresponding to this particular choices of signs is indicated on the right, where only the sign on the nonzero matrix elements is indicated. Note that nonzero connections in the same row have the same sign.

matrix. We now argue that the results presented in this paper are readily extended also to this scenario, which is more realistic for neural networks.

To take this situation into account, we consider (taking $g = 0$ for now)

$$\boldsymbol{G} = \begin{pmatrix} & \sigma_1 & & & & \\ \sigma_2 & & \sigma_2 & & & \\ & \sigma_3 & & \sigma_3 & & \\ & & \sigma_4 & & \ddots & \\ & & & \ddots & & \ddots \\ & & & & \ddots & & \sigma_{N-1} \\ & & & & & \sigma_N & \end{pmatrix} \tag{24}$$

instead of $\boldsymbol{M}$ in Eq. (18), where each of σ_j randomly takes ± 1 with probability $1/2$, although similar considerations apply to the more general probability distribution of Eq. (5). The value of σ_j indicates whether the two connections out of the jth neuron are excitatory or inhibitory.

According to the previous argument, the spectrum depends only on the product of opposing off-diagonal elements. In the case of the matrix (24), we can regard the $N - 1$ quantities $\{\sigma_j \sigma_{j+1} = \pm 1 \| j = 1, 2, \ldots, N - 1\}$ as independent random variables, just as for the matrix of Eq. (18) we can regard the $N - 1$ quantities $\{s_x^+ s_x^- = \pm 1 \| x = 1, 2, \ldots, N - 1\}$ as independent. Therefore, the matrices (18) and (24) are statistically isospectral; see Fig. 6(b) for the spectrum for one random sample, obeying Dale's law, to be compared with Fig. 4(b).

The statistical isospectrality does not change much when we introduce the boundary terms $\boldsymbol{G}_{1N} = \sigma_N$ and $\boldsymbol{G}_{N1} = \sigma_1$, because the perturbation of these terms to the spectrum is of order $1/N$ at most (and exponentially small if the states are localized). The only difference in the statistics is the fact that the product of all super- and subdiagonal elements of the matrix (18), including the boundary terms $\boldsymbol{M}_{1N} = s_N^+$ and $\boldsymbol{M}_{N1} = s_N^-$, is random and can take ± 1, but that of the matrix (24) is always $+1$.

FIG. 6. The spectra on complex planes of (a) the directed matrix (19) with random signs for $g = 0.1$ and $N = 1000$; (b) the matrix (24) obeying Dale's law for $N = 1000$; Note the similarity to the spectrum in Fig. 4(b), that does not have this restriction. (c) the matrix (25) for $g = 0.1$ and $N = 1000$. Note the close similarity with Fig. 6(a).

C. Spectrum of models obeying Dale's law

Figure 7 shows a network with $N = 5$ that respects Dale's law and the signs of the nonzero elements of the corresponding

Finally, introduction of the asymmetry parameter g to $\boldsymbol{G}$ as in

$$
\boldsymbol{G}(g) = \begin{pmatrix}
 & e^g \sigma_1 & & & & & e^{-g}\sigma_1 \\
e^{-g}\sigma_2 & & e^g \sigma_2 & & & & \\
 & e^{-g}\sigma_3 & & e^g \sigma_3 & & & \\
 & & e^{-g}\sigma_4 & & \ddots & & \\
 & & & \ddots & & \ddots & \\
 & & & & \ddots & & e^g \sigma_{N-1} \\
e^g \sigma_N & & & & & e^{-g}\sigma_N &
\end{pmatrix}
\tag{25}
$$

has the same effect as we showed in Sec. II B for the matrix (19); see Fig. 6(c) for a numerical illustration for one random sample. Note the close similarity with Fig. 6(a), for the matrix $\boldsymbol{M}(g)$, which is unconstrained by Dale's law.

III. LOCALIZATION PROPERTIES

We now investigate the localization properties of the model via three different and complimentary routes:

(1) By calculating the participation ratio of eigenmodes obtained via exact diagonalization;

(2) By using the transfer-matrix approach, and the equivalence between the Lyapunov exponents and the inverse localization length;

(3) By numerically calculating the density-of-states (DOS) via exact diagonalization, and inferring the localization length via the Thouless relation [15], as generalized to localization with complex eigenvalues in Ref. [33].

We find analytically that for $g = 0$ and for any u that the localization length is infinite at $\lambda = 0$ (i.e., the inverse localization length κ vanishes at the origin), suggesting a diverging localization length as $|\lambda| \to 0$. Such a divergence is strongly supported by our numerical results. Interestingly, we find that, in contrast to the results of Ref. [33], the dependence κ on $\lambda = x + iy$ in the vicinity of the origin is not isotropic. Through the Thouless relation, which we elaborate on below, we will show that this property is connected to the vanishing DOS at the origin. In the following, we elaborate on the different methods and compare the results.

A. Localization properties from numerical diagonalization

A useful measure of the localization of an eigenvector is its participation ratio, defined as

$$
P \equiv \sum_j |\psi_j|^2 \Big/ \sum_j |\psi_j|^4.
\tag{26}
$$

Indeed, a perfectly localized eigenvector with support only at a single site would have $P = 1$, while a perfectly delocalized one (with $\psi_j = 1/\sqrt{N}$ for every j) has $P = N$. By averaging the participation ratio, or its inverse, we may gain insights into the localization properties of the system. Figure 8 shows the results of numerical diagonalization of 10 000 matrices of dimension 5000×5000, performed on Harvard's "Odyssey" cluster. These matrices are given by Eq. (4), with $f = 1/2$ and $u = 1$.
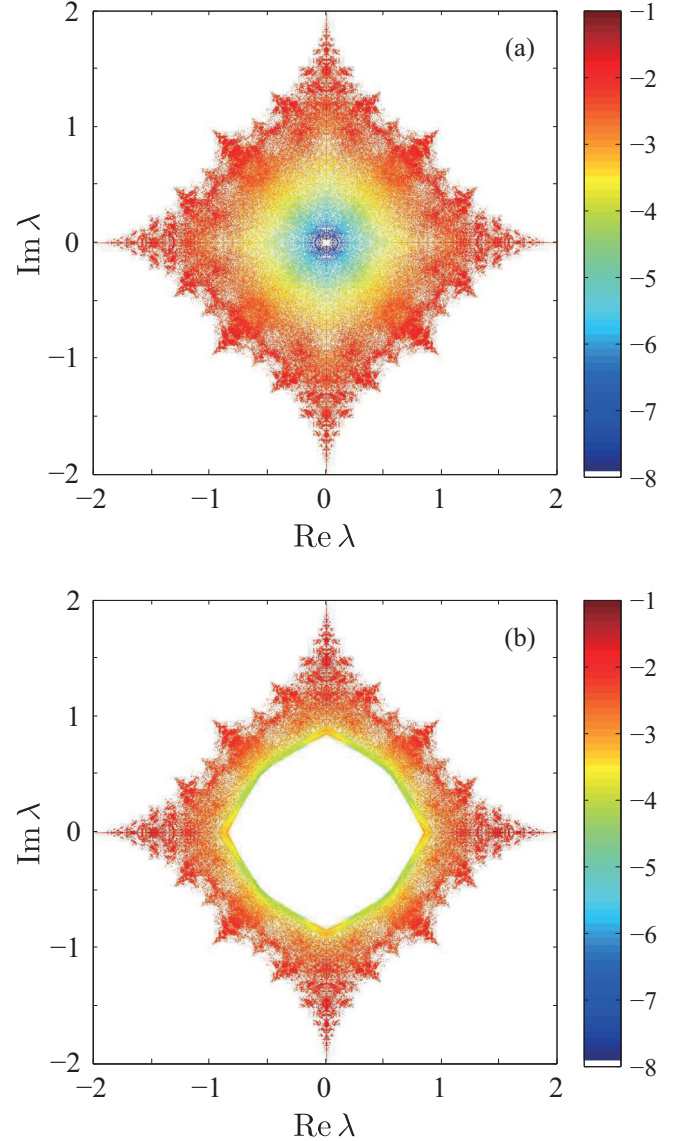

FIG. 8. (a) Inverse participation ratio (IPR) as a function of eigenvalue, obtained via numerical diagonalization of 10 000 matrices of dimension 5000×5000 with $g = 0$ and periodic boundary conditions. With $g = 0$, the results with open boundary conditions would be nearly identical. The color bars indicate the inverse localization length on a logarithmic scale. Note that the background (where there are no states) is white; the fractal nature of the spectrum implies that the IPR is not evaluated everywhere but only on the support of the DOS. (b) IPR for the same parameters but with $g = 0.1$ and periodic boundary conditions. In this case the states become delocalized on the rim of the hole in the DOS.

Figure 8(a) shows the tendency of states to be delocalized near the origin [vanishing inverse localization length (IPR)], becoming more localized away from the origin. However, while this is a direct and straightforward method, in the next Secs. III B and III C, we will find the localization length more accurately; we will show that while it diverges near the origin, it does not have a radial symmetry and only achieves radial symmetry away from the origin.

Upon repeating the analysis for $g = 0.1$ [Fig. 8(b)], we see that the hole in the DOS is accompanied by a diverging localization length on its rim. Later we will show that the model exhibits spectral rigidity: The localized eigenmodes away from the rim of the hole are insensitive to changes in g.

We now comment briefly on the effect of periodic boundary vs open conditions. The arguments given in Sec. II suggest (and numerical diagonalizations confirm) that the $g = 0$ spectrum is nearly identical when periodic instead of open boundary conditions are employed in Fig. 8(a). In contrast, the hole and extended states in the $g = 0.1$ spectrum disappear when periodic boundary conditions are replaced by open boundary conditions in Fig. 8(b). The invariance of spectrum follows from the similarity transformation leading to Eq. (15) of Sec. II, after taking the limits $s_N^+ \to 0$, $s_N^- \to 0$, which breaks the chain. Nevertheless, the hole has a physical interpretation even for open chains: Although all eigenvalues retain their $g = 0$ values, eigenfunctions inside the hole become edge states, piled up on one side of the broken chain.

B. Transfer matrix approach

A well-established method for finding the localization length of a one-dimensional system calculates the Lyapunov exponent via the transfer matrix technique [33]. If ψ_n is the eigenfunction amplitude on the nth site, then the 2×2 transfer matrix connecting the vector $\binom{\psi_n}{\psi_{n+1}}$ to the vector $\binom{\psi_{n-1}}{\psi_n}$ with eigenvalue λ is given by

$$T_n = \begin{pmatrix} 0 & 1 \\ -e^{-2g}s_{n-1}^-/s_n^+ & \lambda e^{-g}/s_n^+ \end{pmatrix}, \qquad (27)$$

where we do not include diagonal disorder and s_{n-1}^- and s_n^+ are independent random variables representing the off-diagonal randomness.

The Lyapunov exponent can be extracted by taking the limit

$$\kappa \equiv \lim_{N \to \infty} \langle \log(||T_N \cdot T_{N-1}...T_1||) \rangle / N, \qquad (28)$$

where $||..||$ denotes the norm of the matrix, and $\langle .. \rangle$ ensemble averaging over the quenched disorder. It can be proven that under quite general conditions the limit exists, and κ equals the inverse of the localization length [35], which we identify (up to constants of order unity) with the inverse participation ratio of Sec. III A.

This procedure provides a numerically attractive route to finding the localization length, without having to diagonalize large matrices. However, in practice, N has to be large in order for the method to be accurate, which implies that the product will result in a matrix with a large norm, imposing computational difficulties. We resolved this problem by working with the recursive relation for the quantity $r_n \equiv \psi_{n+1}/\psi_n$ (note that, unlike in Ref. [33], in our definition r is a complex number). From Eq. (27) we immediately find that

$$r_{n+1} = -(s_{n-1}^-/s_n^+)e^{-2g}/r_n + \lambda e^{-g}/s_n^+. \qquad (29)$$

In this case, the values of r_n are well behaved also for large n, leading to robust numerics. Upon evaluation of $r_1, \ldots, r_N = \psi_{n+1}/\psi_1$, the Lyapunov exponent can be found in a similar
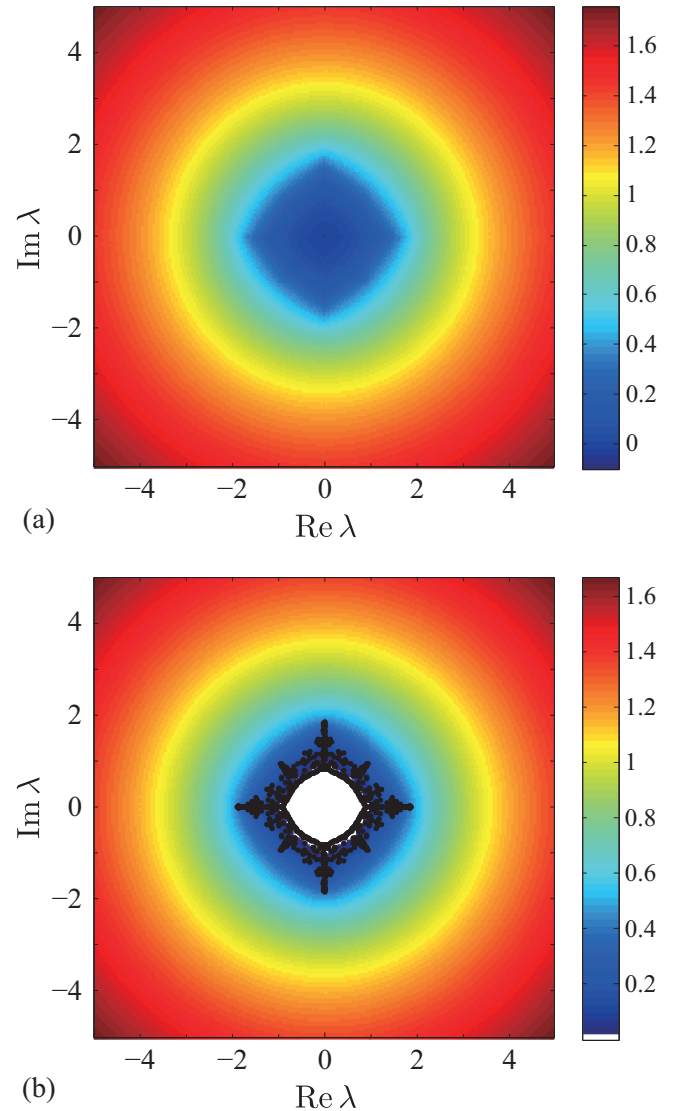

(a)

(b)

FIG. 9. (a) Inverse localization length $\kappa(\lambda)$ as a function of eigenvalue, obtained via Eq. (30) and the recursion equation (29). Each point is obtained via 10 000 iterations. In this case, κ does not take negative values anywhere. (b) The colored map shows $\kappa(\lambda)$ for the same parameters but with $g = 0.1$. There is a finite region in the vicinity of the origin with *negative* values of κ, which was given a white color (not included in the color map). This region corresponds to the gap of Fig. 8(b); the black dots superimposed on the plot are the result of the diagonalization of a single 1000×1000 matrix with $g = 0.1$. Note that the boundary of the white hole corresponds almost exactly to the rim of the extended states found via the exact numerical diagonalization.

fashion as

$$\kappa(\lambda) = \frac{1}{N} \sum_{j=1}^{N} \log |r_j|. \qquad (30)$$

It is beneficial to omit the values of r_j at the beginning of the sequence, to reduce the effects of the initial conditions, though in the limit of large N this is not strictly necessary.

Using this method, we obtained Fig. 9, which corroborates and complements the results of the exact numerical

diagonalization. While Fig. 8 is computationally expensive, generating Fig. 9 takes several minutes on a PC, a testimony to the power of this technique. Note, however, that Eqs. (29) and (30) *always* deliver a value for $\kappa(\lambda)$, regardless of whether there is actually a normalizable eigenfunction at that particular value of λ.

C. Connection to the density-of-states via the Thouless relation

A classic result in the theory of Anderson localization in one dimension is an elegant relation connecting the density-of-states to the localization length, due to Thouless [15]. This relation can readily be generalized to the non-Hermitian case [33], where it states that

$$\nabla^2 \kappa(x,y) = \rho(x,y). \qquad (31)$$

Here the complex eigenvalue is $\lambda = x + iy$, and $\rho(x,y)$ is the density-of-states. This equation can be inverted, using the well-known analogy with 2D electrostatics, whereby $\rho(x,y)$ represents a collection of infinite, charged wires, perpendicular to the complex plane, each associated with a logarithmic potential. Therefore we have

$$\kappa(x,y) = \int \rho(x',y') \log(|r - r'|) dx\, dy + C. \qquad (32)$$

In the case $g = 0$, the constant is given by [37]

$$C = \langle \log(|s_j^+|) \rangle = \langle \log(|s_j^-|) \rangle, \qquad (33)$$

i.e., the average of the logarithm of the random matrix elements. Hence, in the case where we are focusing on where $|s_j^+| = 1$, we find that $C = 0$. In the next section we shall show how the results for $\kappa(x,y)$ for finite g can be mapped to the $g = 0$ behavior, which will show that in the more general case we have

$$C = \tfrac{1}{2} \langle \log(|s_j^-/s_j^+|) \rangle = -g, \qquad (34)$$

which follows from Eq. (37).

This remarkable relation allows us to go back and forth between the two very different numerical procedures: obtaining κ via the recursion relation and obtaining ρ via exact numerical diagonalization. Indeed, using a *single* realization of a 1000×1000 matrix and applying this formula allows us to recover the Lyapunov exponent dependence on energy, shown in Fig. 10 for the case $g = 0$.

D. Hole in spectrum corresponds to contours of Lyapunov exponent

Consider the recursion relation of Eq. (29). It is easy to "gauge away" the effect of g by making the transformation

$$y_n \equiv r_n e^g, \qquad (35)$$

upon which the equation takes the form

$$y_{n+1} = -\left(\frac{s_{n-1}^-}{s_n^+}\right) \Big/ y_n + \lambda/s_n^+. \qquad (36)$$

This representation implies that for any complex eigenvalue $\lambda = x + iy$, the effect of g is to decrease the Lyapunov exponent by an amount g:
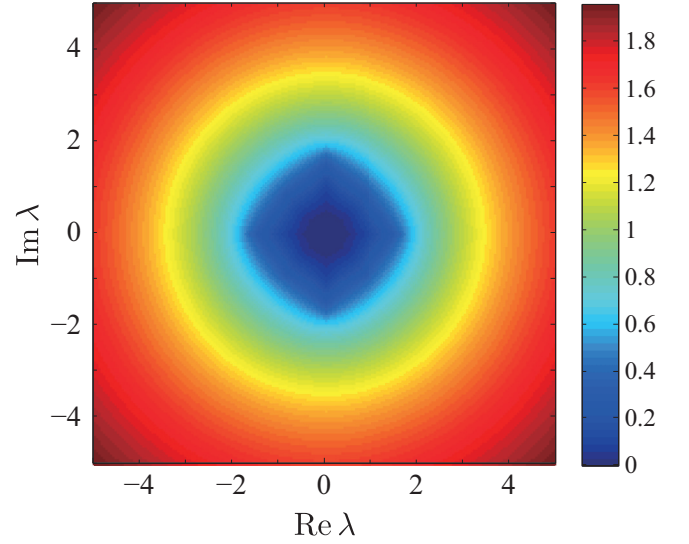
$$\kappa(x,y;g) = \kappa(x,y;0) - g. \qquad (37)$$

FIG. 10. The Lyapunov exponent $\kappa(\lambda)$ was extracted from the diagonalization of a single 1000×1000 matrix with $g = 0$, using the electrostatic relation (32). The result is very similar to Fig. 9(a), which was obtained via the Ricatti recursion relations.

Hence, consistent with the gauge transformation result of Eq. (23), for any $g > 0$ all states which previously had $\kappa < g$ will acquire a *negative* Lyapunov exponent. Since all states must be normalizable, the region with negative κ will not support any eigenfunctions and corresponds to the "hole" or gap seen in Figs. 2 and 6. This argument implies that the hole boundary corresponds to contour where $\kappa = g$, consistent with Fig. 9(b), where the results of exact diagonalization are superimposed on top of the Lyapunov exponent heatmap.

In Fig. 11, the contours of constant κ are shown. As expected from the electrostatic Thouless relation, away from the effective support of the DOS the contours become circular, $\kappa(x,y) \propto \log(x^2 + y^2)$, since all "charges" associated with the complex eigenvalues act as if they were concentrated at the origin. Close to the origin the contours obtain a roughly diamond or octagonal shape. This behavior is consistent with
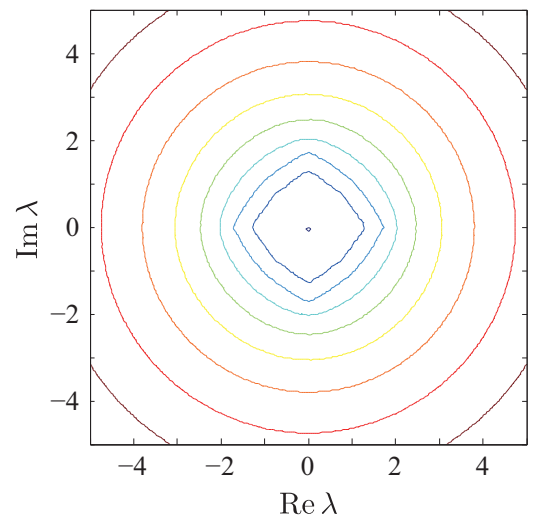

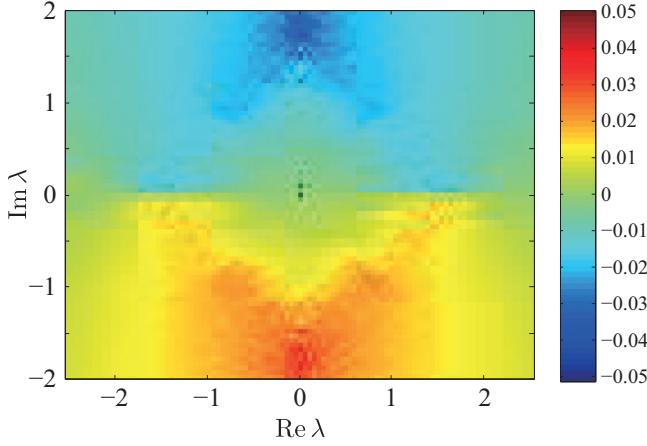FIG. 11. Constant κ contours of the heatmap of Fig. 9(a).

FIG. 12. The y component of the gradient of the Lyapunov exponent. The abrupt change along the x is consistent with a condensation of eigenvalues along the real axis.

FIG. 13. Numerically extracted contours of constant Lyapunov exponent near the origin, compared with those of Eq. (38).

the vanishing DOS suggested by Fig. 2(a); via the Thouless relation, Eq. (31), if κ had a perturbative expansion such as $\kappa \sim x^2 + y^2$ (see Ref. [33] for such result in a related model), then the DOS at the origin would have a finite, nonvanishing value.

Furthermore, Fig. 12 shows the results for the y component of the *gradient* of the Lyapunov exponent, suggesting a δ-function contribution to the DOS along the x axis. Similar results can be obtained for the y axis. For $u = 1$, the strength of the singular DOS along the x and y axis decays *linearly* close to the origin, as shown in Fig. 3. These results lead us to the following ansatz for the behavior of κ near the origin for $u = 1$:

$$\kappa(x,y) \sim (|x| + |y|)\sqrt{x^2 + y^2}, \qquad (38)$$

i.e., it is a product of L_1 and L_2 norms. This ansatz is consistent with the eigenvalue condensations onto the x and y axes and their linear density shown in Fig. 3. When appropriate higher-order cubic terms are added to the ansatz of Eq. (38), the function becomes harmonic away from the x and y axes (e.g., by replacing $d = \sqrt{x^2 + y^2}$ with $[1 - e^{-2d}]$), consistent with the vanishing DOS at the origin. The good agreement of the equipotential contours of the ansatz of Eq. (38) and of the numerically evaluated Lyapunov exponent is shown in Fig. 13.

E. Vanishing of the Lyapunov exponent at the origin

It is easy to see that for *any* distribution of the hopping matrix elements, the Lyapunov exponent must vanish at the origin (in contrast to the behavior of models with additional diagonal disorder [37]). To see this, consider the transfer matrix Eq. (27) for $\lambda = 0$. The product of two adjacent transfer matrices is in this case diagonal:

$$S_n = T_n T_{n-1} = e^{-2g} \begin{pmatrix} -\frac{s_{n-1}^-}{s_n^+} & 0 \\ 0 & -\frac{s_{n-2}^-}{s_{n-1}^+} \end{pmatrix}, \qquad (39)$$

with the elements on the diagonal being the *ratio* of two random variables. Therefore the Lyapunov exponent is
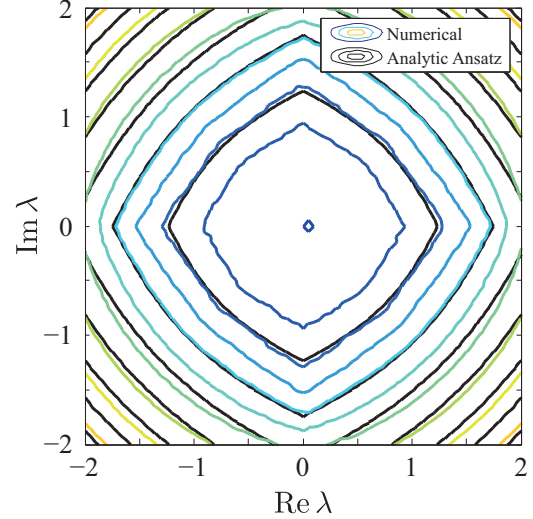
given by

$$\kappa = \tfrac{1}{2}\langle \log(|s_j^- / s_j^+|) \rangle = 0, \qquad (40)$$

a result that holds provided that s_j^- and s_{j+1}^+ are chosen from identical, independent probability distribution functions, as in Eq. (5). The vanishing value of κ at the origin is numerically corroborated in Fig. 9. In fact, for $\lambda = 0$ [and for any probability distribution function $P(s)$], there is an extended eigenfunction of Eq. (4) that reads

$$|\lambda = 0, g = 0\rangle = |1\rangle + \sum_{m=1}^{(N-1)/2} (-1)^m \frac{s_1^- s_3^- \ldots s_{2m-1}^-}{s_2^+ s_4^+ \ldots s_{2m}^+} |2m + 1\rangle$$

$$\equiv |1\rangle + \sum_{m=1}^{(N-1)/2} \psi_m |2m + 1\rangle,$$

$$\psi_m = (-1)^m \frac{s_1^- s_3^- \ldots s_{2m-1}^-}{s_2^+ s_4^+ \ldots s_{2m}^+}, \qquad (41)$$

where we have assumed N is odd and the amplitudes on all even sites vanish. A similar state can be constructed for an even number of sites, with a mild restriction on s_N^+ and s_N^- in both cases when periodic boundary conditions are imposed. That this zero energy state is indeed extended follows from the definition of the inverse localization length within the transfer matrix method [26–29], $\kappa = \lim_{N\to\infty} \frac{1}{N}\langle \log |\psi_N| \rangle$, where the average is over the probability distributions of the matrix elements in Eq. (41).

F. Spectral rigidity outside the gap

Consider the model for $g = 0$, and "ramp up" g. As we argued in Sec. III D and as was discussed in Ref. [37] in the context of a related model, this results in a hole that tracks the contours of constant Lyapunov exponent. Thus, as g increases, the hole widens and "sweeps away" the eigenvalues in its vicinity. The hole hence acquires a finite fraction of the spectrum, concentrated on its one-dimensional rim. Since the
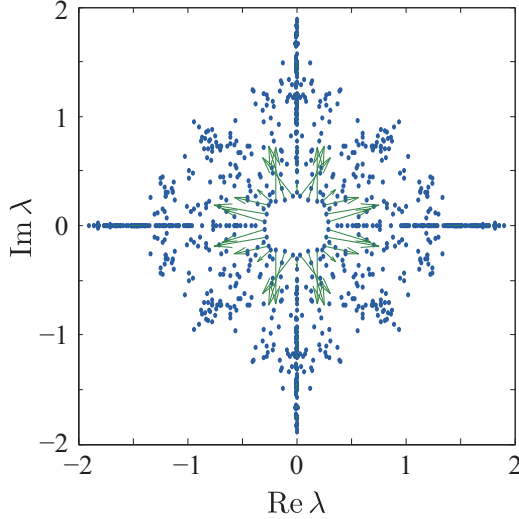
FIG. 14. The eigenvalues of an exact numerical diagonalization of a matrix with $N = 1000$, $g = 0.01$ (blue dots). From each point a line emanates, in the direction of the eigenvalue velocity in the complex plane (*i.e.* $\frac{d\lambda}{dg}$), and with length proportional to the velocity. For eigenvalues away from the rim of the hole, no line is visible; spectral rigidity implies vanishing velocities in this regime.

rim of the hole corresponds to diverging Lyapunov exponent, these states have all become *delocalized* by the finite value of g, while the states outside the hole are still localized, as explained in Sec. II B. These states are insensitive to the boundary conditions, and their eigenvalues will not be modified by g.

This spectral rigidity is illustrated in Fig. 14. To calculate the eigenvalue velocity $d\lambda/dg$, we used first-order perturbation theory, which states that this derivative is given by

$$\frac{d\lambda}{dg} = \frac{dx}{dg} + i\frac{dy}{dg} = \left(\vec{v}_\lambda^L, \boldsymbol{B}\vec{v}_\lambda^R\right), \qquad (42)$$

where $\vec{v}_\lambda^R >$ and $\vec{v}_\lambda^L$ are the right and left eigenvectors, respectively, of the non-Hermitian matrix $\boldsymbol{M}(g)$, $(...,...)$ is the scalar product, and the matrix $\boldsymbol{B}$ is the matrix derivative of the matrix $\boldsymbol{M}(g)$ with respect to g.

IV. PERTURBATION THEORY FOR LARGE g

Our problem simplifies for large g. In this limit we first neglect all terms of order e^{-g}, and the remaining matrix, with periodic boundary conditions, is of the form (illustrated for $N = 4$)

$$\boldsymbol{M} = \begin{pmatrix} 0 & s_1^+ e^g & 0 & 0 \\ 0 & 0 & s_2^+ e^g & 0 \\ 0 & 0 & 0 & s_3^+ e^g \\ s_4^+ e^g & 0 & 0 & 0 \end{pmatrix} \qquad (43)$$

with $s_j^+ = \pm 1$ for $f = 1/2$ and $u = 1$. We can attempt to "gauge out" the signs of $\{s_j^+\}$ by applying a similarity transformation $H = Q^{-1}MQ$ with

$$\boldsymbol{Q} = \begin{pmatrix} c_1 & 0 & 0 & 0 \\ 0 & c_2 & 0 & 0 \\ 0 & 0 & c_3 & 0 \\ 0 & 0 & 0 & c_4 \end{pmatrix}. \qquad (44)$$

Choosing $c_1 c_2 = s_1^+, c_2 c_3 = s_3^+ \cdots c_n c_1 = s_n^+$ (with each $c_i = \pm 1$) results in a matrix of the form

$$\boldsymbol{H} = e^g \begin{pmatrix} 0 & 1 & 0 & 0 \\ 0 & 0 & 1 & 0 \\ 0 & 0 & 0 & 1 \\ 1 & 0 & 0 & 0 \end{pmatrix}. \qquad (45)$$

Note that $\boldsymbol{H}$ is proportional to the translational operator for a clockwise rotation of one lattice constant around the ring. This procedure can only be applied when the product of the odd elements $s_1^+ s_3^+ \ldots$ equals that of the even elements $s_2^+ s_4^+ \ldots$ (which occurs with probability $1/2$). If this is not the case, however, then a similar approach can still be pursued (with purely imaginary value of $\{c_i\}$ in this case) leading to similar results.

This matrix is readily diagonalized by plane waves, i.e., right eigenvectors $v_j^R = e^{ikj}$, where the periodic boundary conditions imply that the allowed values of k must be $k = 2\pi n/N$, $n = 0, 1 \cdots (N-1)$; note that the left eigenvectors are given by $v_j^L = e^{-ikj}$. The resulting eigenvalues are then

$$\lambda_k = e^{g+ik}, \qquad (46)$$

i.e., except for their magnitude e^g they are the N roots of unity. The eigenvectors of the original matrix $\boldsymbol{M}$ are plane waves modulated by random sign changes determined by the elements s_j^+.

So far we concluded that to zeroth order the eigenvalues will sit at *regular intervals on a circle*. We may now introduce the terms with the factor e^{-g} as a perturbation and calculate the shift of the eigenvalues to the first order in perturbation theory. The perturbation matrix is of the form (both before and after the similarity transformation)

$$\boldsymbol{B} = e^{-g} \begin{pmatrix} 0 & 0 & 0 & s_4^- \\ s_1^- & 0 & 0 & 0 \\ 0 & s_2^- & 0 & 0 \\ 0 & 0 & s_3^- & 0 \end{pmatrix}. \qquad (47)$$

Within first-order perturbation theory the shift in the kth eigenvalue is

$$\delta\lambda_k = \left(\vec{v}_k^L, \boldsymbol{B}\vec{v}_k^R\right), \qquad (48)$$

and upon inserting the plane-wave eigenfunctions we have

$$\delta\lambda_k = e^{-g}[e^{-ik}(s_1^- + s_2^- \cdots + s_{n-1}^- + s_N^-)/N], \qquad (49)$$

Upon invoking the central-limit theorem, for large N we can replace the sum by a Gaussian variable with variance N. Hence the eigenvalue will be shifted in the direction $\pm 1/\lambda$, with a magnitude of order $e^{-g}/\sqrt{N}$. Note that the magnitude of the shift is identical for all eigenvalues. These results are illustrated in Fig. 15.

It is straightforward to repeat these calculations for hopping elements s_j^+ and s_j^- governed for the more general probability distribution of Eq. (5). After a similarity transformation, $M \to M' = P^{-1}MP$, with $P = \text{diag}\{1, 1/s_1^+, 1/(s_1^+ s_2^+), \ldots\}$ and up to corner matrix elements that do not affect our results as
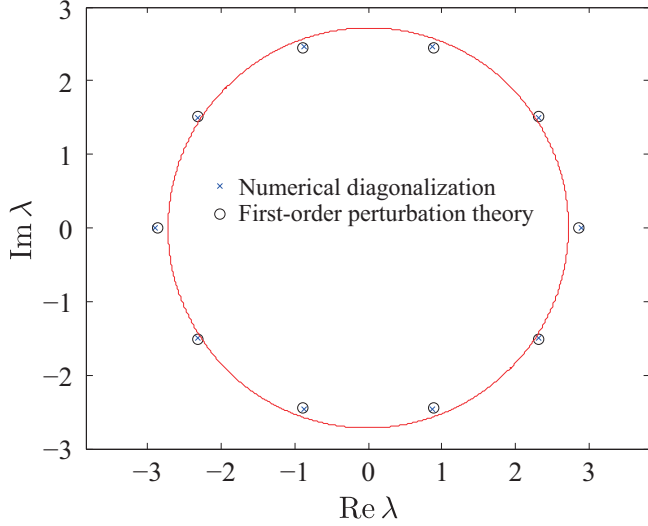
FIG. 15. Comparison of first-order perturbation theory and exact numerical diagonalization, for $g = 1$, $N = 10$. The red circle has radius e^g.

$N \to \infty$, we have

$$\boldsymbol{M'} = -\sum_{j=1}^{N}[e^g|j+1\rangle\langle j| + s_j^+ s_j^- e^{-g}|j\rangle\langle j+1|]$$

$$\equiv \boldsymbol{H} + \boldsymbol{B}, \tag{50}$$

where the periodic boundary conditions imply $|j+N\rangle = |j\rangle$. We recover the plane-wave eigenvectors discussed above for H and find, from first-order perturbation theory,

$$\langle \lambda_k \rangle = e^{g+ik} + e^{-g-ik}\frac{1}{N}\sum_{j=1}^{N} s_j^+ s_j^-. \tag{51}$$

With the help of the probability distribution of Eq. (5), we can now carry out a disorder average, with the result

$$\lambda_k = e^{g+ik} + e^{-g-ik}(1+u)^2(f-1/2)^2$$

$$\equiv e^{g+ik} + \alpha e^{-g-ik}, \alpha = (1+u)^2(f-1/2)^2, \tag{52}$$

so the eigenvalues will lie on an ellipse with major axis $e^g + \alpha e^{-g}$ and minor axis $e^g - \alpha e^{-g}$. It is straightforward to show for this generalized problem that the fluctuation of the kth eigenvalue about its mean values is $O(e^{-g}/\sqrt{N})h(u,f)$, where $h(u,f)$ is a dimensionless function of order unity.

In Appendix C, we go to *second* order in perturbation theory and show that it leads to a similar picture qualitatively.

V. SUMMARY AND OUTLOOK

In this paper we studied a coarse-grained, simplified model for the dynamics of neural networks, which, upon linearization close to a steady state, leads to the study of the eigenvector spectrum of an ensemble of sparse, non-Hermitian matrices. In contrast to most previous studies in this context, here the connections were only between neighboring neurons, i.e., the model included a spatial structure. For concreteness and simplicity, we focused on a ring topology, which is realized in several instances in neuroscience [39,40]. An additional
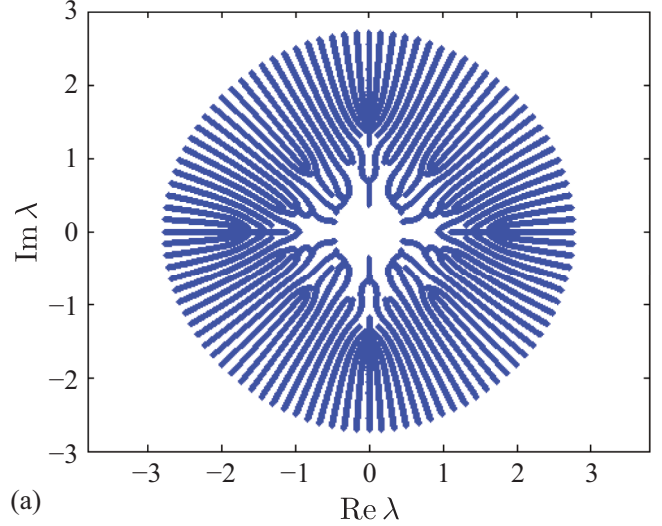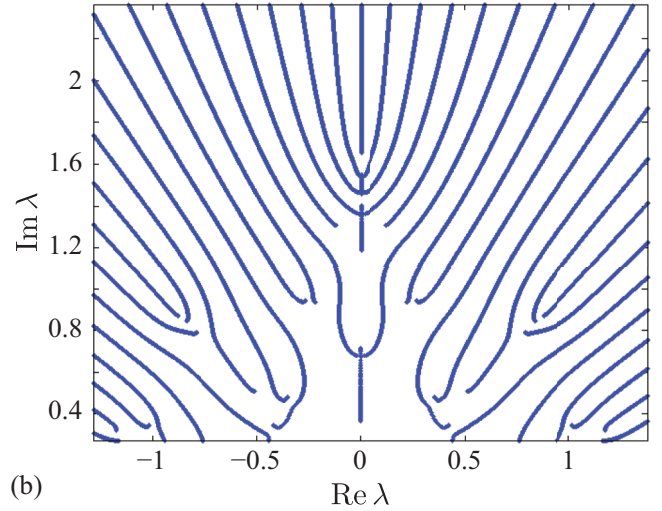
FIG. 16. Plot of the eigenvalues of a particular $N = 100$ matrix, where g is varied continuously from 1 (corresponding to the outer circle) down to 0. These eigenvalues stop changing with g when their eigenfunctions localize. (b) is an enlarged view of a part of (a).

parameter in our model, g, controlled the directional bias in the neural network, i.e., favoring clockwise over counterclockwise connections.

Despite the deceptive simplicity of the model, it exhibits surprisingly rich behavior both in terms of the eigenvalue spectrum and in terms of the localization properties of the eigenvectors. Figure 16 shows the trajectories of eigenvalues for a particular instance $N = 100$ and for a value of g decreasing from one down to zero. The eigenvalues "flow" in the complex plane until their motion ultimately ceases once the corresponding eigenvectors become localized. For large values of g, we used perturbation theory to show that the eigenvectors are approximately plane waves (up to a similarity transformation) and that the eigenvalues form a circle (or an ellipse, more generally) in the complex plane. As g decreases, eigenvalues move in the complex plane until they localize, after which "spectral rigidity" will take over and the motion of the localized eigenvalue stops. The final positions of the
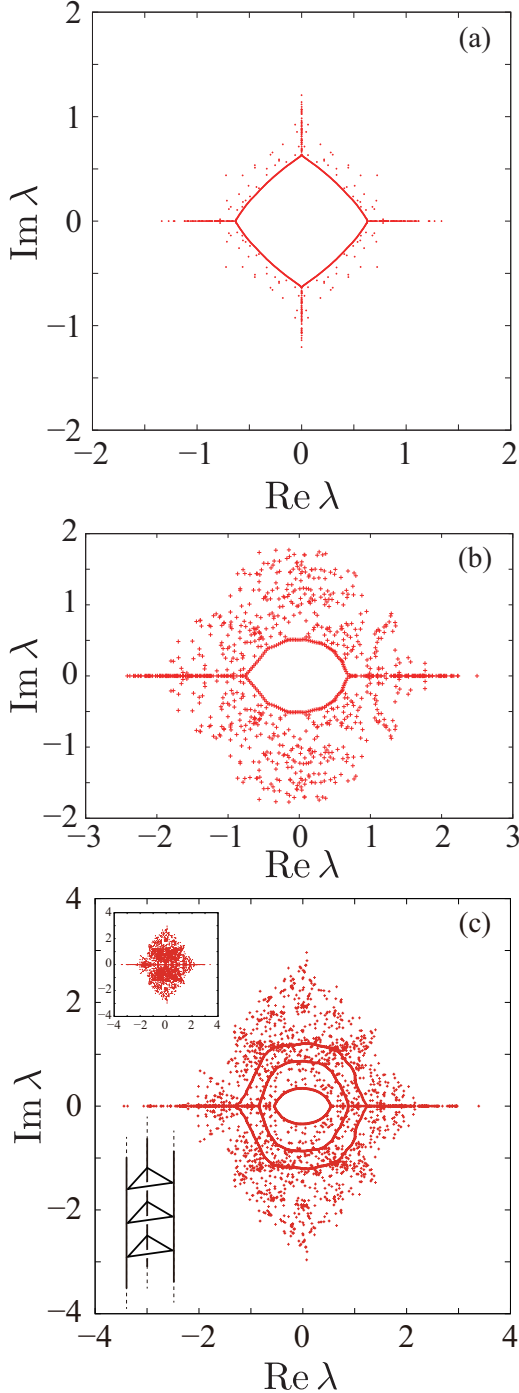
FIG. 17. (a) Single-box ($u = 0$) spectrum with $N = 1000$ and $g = 0.5$. A macroscopic fraction of eigenvalues still condensed onto the real and imaginary axes (compare Fig. 2), but the remaining eigenvalues now have a diamondlike boundary. A diamond-shaped gap now replaces the octagonal hole in Fig. 2(b). (b) Spectrum for the bimodal model with symmetrical diagonal randomness with elements d_j chosen from a uniformly from the interval $[-1,1]$, with $N = 1000$ and $g = 0.1$. Although only the real axis now has a macroscopic fraction of the eigenvalues, a lens-shaped gap replaces the octagonal hole in Fig. 2(b). (c) Spectrum for a ladder of 1000 stacked triangles (see sketch at lower left), with periodic boundary conditions and all 3000 connections obeying Dale's law with randomly chosen strengths ± 1. The asymmetry parameter $g = 0.2$ for the central spectrum, with $g = 0$ in the inset at upper right. Eigenvalues no longer condense onto

eigenvalues for $g = 0$, when this game of "musical chairs" has ended, showed a remarkably intricate, fractal-like pattern [26]. For any intermediate value of g, the spectrum will show a pronounced "hole" or gap surrounding the origin, with the eigenvalues which will ultimately end inside the hole lying on its boundary, and with localized states outside it.

The spectra of conventional, highly connected random matrices for large N can be grouped into universality classes, such as those of the Gaussian orthogonal ensemble and the Gaussian unitary ensemble, and those obeying the circular law [1]. It is natural to ask about the universality of the spectra and eigenfunctions of the one-dimensional sparse random matrices studied here. Because of its beautiful fractal-like spectrum, we have focused here on directed localization in the bimodal non-Hermitian random hopping model of Feinberg and Zee [26]. However, many of our conclusions also apply to the more general model defined by Eqs. (4) and (5). For example, the symmetries under reflections across the real and imaginary axes and under $90°$ rotations in the complex plane discussed in Sec. II are preserved for arbitrary u when $f = 1/2$. As discussed in Sec. III E, there is always a divergent localization length at the origin in this model. As summarized in Appendix B, when $f = 1/2$, approximately equal numbers of the eigenvalues ($\sim$40–70% total) condense onto the real and imaginary axes when $g = 0$, as u varies from a bimodal distribution ($u = 1$) to a symmetric double-box distribution ($0 < u < 1$) to a symmetric single-box distribution ($u = 0$). As f moves away from $1/2$, we expect that the spectrum becomes more elliptical, consistent with the eigenvalue spectrum derived in the large g limit in Eq. (52). Another aspect of universality, which connected with Dale's law in neuroscience, was addressed in Sec. II C.

The gauge transformation argument leading to Eq. (37) is quite general. Provided the localization length increases monotonically at the origin, it predicts for 1D rings a gap or hole bounded by a rim of extended states in the spectrum for $g > g_{c_1}$. Because the localization length diverges at the origin for the model defined by Eqs. (4) and (5), we expect that $g_{c_1} = 0$ in this case. When diagonal disorder is present, the localization length for $g = 0$ remains finite even at the origin and now $g_{c_1} > 0$ [37]. To illustrate the universal nature of the gap, Fig. 17 shows a single-box ($u = 0$) spectrum with $N = 1000$ and $g = 0.5$ and a spectrum for the bimodal model with symmetrical diagonal randomness with elements d_j chosen from a uniform distribution with support $[-1,1]$, with $N = 1000$ and $g = 0.1$. Although the single-box spectrum in Fig. 17(a) no longer has the fractal-like eigenvalue spectrum shown in Fig. 2, a diamond-shaped gap centered on the origin with an enhanced density of states is clearly present. In Fig. 17(b), we see that diagonal randomness added to the bimodal model destroys the symmetry under $90°$ rotations by removing the eigenvalue condensation onto the imaginary

FIG. 17. (*Continued*) the imaginary axis, similarly to (b). A hole or gap in the spectrum again appears centered on the origin, bordered by extended states. Although the states condensed into the two outer rings are also extended, states outside the outermost ring remain localized.

axis. Nevertheless, a hole in the spectrum with an enhanced density of states on its rim survives the imposition of diagonal randomness for this value of $g = 0.1 > g_{c_1} > 0$. The large g perturbation theory of Sec. IV can be used to show that all states are delocalized (being plane-wave like) as $g \to \infty$ for a wide class of models, including those with diagonal randomness. Hence, we expect that there exists another critical value g_{c_2}, such that for $g > g_{c_2}$ all states are delocalized. Localized eigenfunctions in neuroscience could be helpful for avoiding crosstalk between different neural computation centers, and the extended states on the rim of the hole when $g > 0$ might be used to transmit information over longer distances.

As discussed in the Introduction, a connection with real neural networks is facilitated if each node in our simplified one-dimensional model is regarded as a coarse graining of a cluster of strongly coupled neurons, randomly chosen to be inhibitory or excitatory. A systematic study of one-dimensional rings of randomly coupled neural clusters, with each cluster in isolation exhibiting, say, a "circular law" due to internal connections [5,6], is beyond the scope of this paper. However, Fig. 17(c) shows that essential elements of our results are preserved in the simple case of a ring formed from three-neuron triangles. As sketched in the bottom inset, imagine a stack of triangular clusters are connected to form a 1000-cluster ring with periodic boundary conditions, with a triplet of connection pairs between adjacent triangles. Every node is randomly chosen to be purely excitatory or inhibitory, with all these non-Hermitian connections (either within triangles or connecting neighboring triangular clusters) of strength ± 1, similar to the implementation of Dale's law summarized in Fig. 7. The spectrum in Fig. 17(c), which has a clockwise bias $g = 0.2$ on the connections between triangles, exhibits the same hole in the density of states found for simple rings, with extended states again piled up on the edge of the rim. (The spectrum for $g = 0$ with an otherwise identical realization is shown as an inset in the upper right.) Although eigenvalues still condense onto the real axis, this condensation is now absent on imaginary axis, similarly to the case of diagonal randomness shown in Fig. 17(b). Imagine coarse-graining triangle ladders by diagonalizing the individual triangles and then re-expressing the matrix in terms of these basis functions. Diagonal randomness (albeit with complex entries) will in fact appear in this new description, similarly to the case of simple diagonal randomness embodied in Fig. 17(b). Especially intriguing are the two additional, approximately hexagonal, condensations of eigenvalues beyond the hole in Fig. 17(c). A hole with three similarly nested rings of eigenvalues, all with smaller size, appears for $g = 0.1$. Because these rings move as g varies, they are sensitive to boundary conditions and hence likely to be populated with extended states. Other eigenvalues (such as those outside the largest ring) do not move with g and hence correspond to localized states. The support of the spectrum associated with P isolated neurons randomly coupled to form an isolated cluster presumably occupies a region of order $\sqrt{P}$ in the complex plane [5,6]. For Q balanced excitatory and inhibitory connections between clusters coupled together to form a ring, the effective connection strength presumably scales like $\sqrt{Q}$. It would be interesting to test these conjectures and to explore the implications of the bands of extended and localized states shown in Fig. 17(c) for network dynamics.

Although we focus here on applications to sparse neural networks, similar non-Hermitian random matrix problems arise when random ecological networks [41–43] are adapted to allow for spatial structure, with predator and prey species localized to an array of lattice sites but allowed to interact with their neighbors. For example, a site dominated by foxes would have an inhibitory effect on neighboring sites occupied by rabbits, whereas rabbits would have an excitatory effect on nearby foxes. Random excitatory and inhibitory connections in one dimension could also be studied in chains of artificial cells with spatially coupled gene expression patterns [44].

APPENDIX A: SPECTRUM OF THE HERMITIAN RANDOM-HOPPING MODEL

It is interesting to contrast our model of non-Hermitian localization with its Hermitian analog, which also has a diverging localization length at the origin and a connection between the density-of-states and the inverse localization length. The Hermitian random hopping model we consider is a reformulation of Eq. (1),

$$\boldsymbol{H}_{\mathrm{Herm}} = -\frac{1}{2}\sum_{j=1}^{N} t_j(|j+1\rangle\langle j| + |j\rangle\langle j+1|), \quad \text{(A1)}$$

where $\{t_j\}$ is a set of mutually independent random variables taking the values in the range $[1 - \Delta, 1 + \Delta]$ with $0 \leqslant \Delta < 1$. Although this is a standard one-dimensional version of the Anderson model [8,14], dominated by localized eigenstates, it is well established [45,46] that the state at $\lambda = 0$ is *delocalized* with both the localization length and the density-of-states diverging as $|\lambda| \to 0$.

Figure 18 illustrates the density-of-states $\rho(\lambda)$ and the inverse localization length $\kappa(\lambda)$ for $\Delta = 0.85$. We numerically confirmed that the Hermitian version of the Thouless formula connects these quantities [15]:

$$\kappa(\lambda) = P \int_{-\infty}^{\infty} d\lambda' \rho(\lambda') \log|\lambda - \lambda'|, \quad \text{(A2)}$$

where P denotes the principal part. We can indeed see evidence for singularities around $\lambda = 0$ in both figures. These singularities are expected to take the forms [14]

$$\rho(\lambda) \sim \frac{1}{|\lambda|\log^3(1/|\lambda|)}; \quad \text{(A3)}$$

$$\kappa(\lambda) \sim 1/\log(1/|\lambda|). \quad \text{(A4)}$$

TABLE I. The fraction of the states on the real and imaginary axes as well as of the states with the zero eigenvalue. The data in the row "binomial" are for the binomial distribution ± 1 of 1000 samples of length 1000, the data in the next four rows are for the two-box distribution of 500 samples of length 1000, and the data in the last row are for the one-box distribution $[-1,1]$ of 500 samples of length 1000.

Distribution	On real axis	On imaginary axis	Zero eigenvalues
Binomial ($u = 1$)	19.9%	19.9%	0
$u = 0.95$	19.8%	20.0%	0
$u = 0.75$	20.4%	20.6%	0
$u = 0.5$	21.8%	21.9%	0
$u = 0.25$	24.7%	24.8%	66 (0.013%)
One box ($u = 0$)	33.7%	33.8%	792 (0.16%)

eigenvalue states would be extended if they existed for the binomial distribution, as is shown in Sec. III E. The density-of-states looks noisy for the binomial distribution; this may reflect the fractality of the spectrum. However, it becomes smooth for $u \leqslant 0.5$ and at the same time develops a peak around $\lambda = 0$.

APPENDIX C: PERTURBATION THEORY OF THE SIGN-RANDOM TIGHT-BINDING CHAIN

We summarize here second-order perturbation theory applied to our model with $f = 1/2$, $u = 1$, for large g. Upon adopting the similarity transformation of Eq. (9),

$$\boldsymbol{T}_{jj} = \prod_{k=1}^{j-1} \frac{1}{b_k}, \tag{C1}$$

we can bring the tridiagonal hopping matrix

$$\boldsymbol{M}(g) = \begin{pmatrix} & s_1^+ e^g & & & s_N^- e^{-g} \\ s_1^- e^{-g} & & s_2^+ e^g & & \\ & s_2^- e^{-g} & & & \\ & & \ddots & \ddots & \\ & & & & s_{N-1}^+ e^g \\ s_N^+ e^g & & & s_{N-1}^- e^{-g} & \end{pmatrix} \tag{C2}$$

into the form

$$\boldsymbol{M}'(g) = T^{-1} \boldsymbol{M}(g) T$$
$$= \begin{pmatrix} & e^g & & & r_N e^{-g} \\ r_1 e^{-g} & & e^g & & \\ & r_2 e^{-g} & & & \\ & & \ddots & \ddots & \\ & & & & e^g \\ e^g & & & r_{N-1} e^{-g} & \end{pmatrix}, \tag{C3}$$
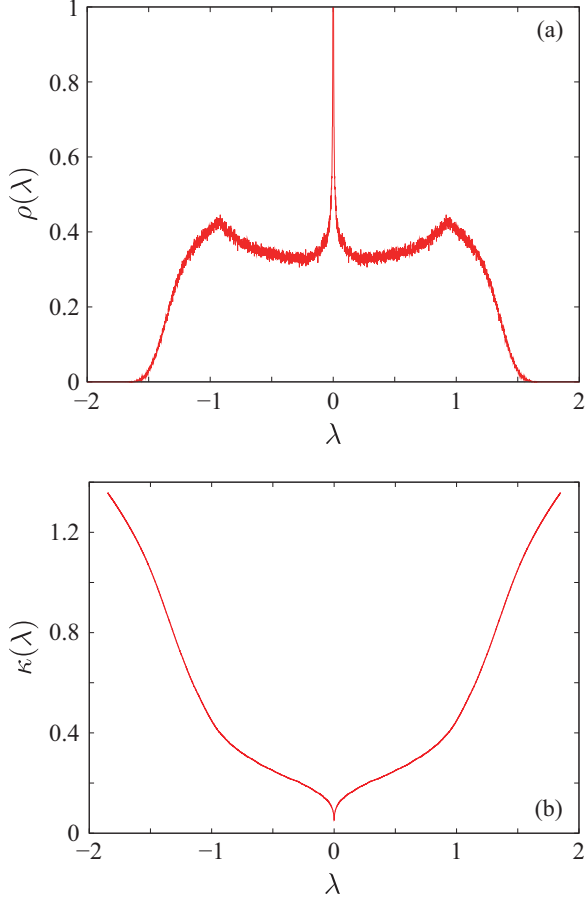
FIG. 18. (a) The density-of-states $\rho(\lambda)$ and (b) the inverse localization length $\kappa(\lambda)$ for a Hermitian ring of length 1000 with hopping randomness. We computed the former from the histogram of the eigenvalues that we obtained from exact diagonalization of 5000 random samples, while the latter from a new algorithm [47] exploiting the Chebyshev-polynomial expansion [48–50] applied to 100 random samples.

APPENDIX B: DENSITY-OF-STATES ON THE REAL AND IMAGINARY AXES FOR $f = 1/2$ AND ARBITRARY u

In this Appendix we study the density of eigenstates that have condensed on the real and imaginary axes for the model defined by Eqs. (4) and (5) with $f = 1/2$ and $g = 0$ as a function of u. For numerical purposes, we here define the states to lie on the real and imaginary axes provided

$$|\operatorname{Im} \lambda_n| < 10^{-8}, \tag{B1}$$

$$|\operatorname{Re} \lambda_n| < 10^{-8}. \tag{B2}$$

We list the fraction of the eigenvalues that satisfy these conditions in Table I, where the zero eigenvalues are the states that satisfy both criteria. As discussed in Sec. III, these states play an important role in determining how $\kappa(x,y)$ vanishes near the origin.

In all cases, the density-of-states (see Fig. 19) is statistically the same on the real and imaginary axes. The zero eigenvalues are absent until the two-box distribution [Eq. (5), $0 < u < 1$] becomes close to the one-box distribution ($u \lesssim 1$). The zero-

FIG. 19. The density-of-states for $f = 1/2$, $g = 0$ on the real axis (filled light blue bars) and on the imaginary axis (open red bars) plotted as histograms $N(\lambda)$: (a) binomial distribution ($u = 1$); (b) $u = 0.95$; (c) $u = 0.75$; (d) $u = 0.5$; (e) $u = 0.25$; (f) one-box distribution ($u = 0$). The system size is 1000 for all data and the number of samples is 500 for all data except for (a), where it is 1000.

where all remaining matrix elements in Eqs. (C2) and (C3) are zero,

$$r_j = s_j^+ s_j^-, \quad j = 1, \ldots, N, \tag{C4}$$

and we have assumed $\prod_{j=1..N} s_j^+ = 1$ in order to get simplified corner matrix elements. The elements r_j are positive or negative random numbers if s_j^+ and s_j^- are random and both positive and negative; in particular, when s_j^+ and s_j^- are ± 1, we have $r_j = \pm 1$ as well. The matrices $\boldsymbol{M}(g)$ and $\boldsymbol{M}'(g)$ are then isospectral.

We now split the matrix $\boldsymbol{M}'(g)$ into the matrix with elements proportional to e^g and the matrix with the elements proportional to e^{-g} and formulate the perturbation of the spectrum of the former with respect to the latter. We thus set $\boldsymbol{M}'(g) = \boldsymbol{M_0} + \boldsymbol{M_1}$, where

$$\boldsymbol{M_0} = e^g \begin{pmatrix} 0 & 1 & & & & \\ & 0 & 1 & & & \\ & & \ddots & \ddots & & \\ & & & 0 & 1 & \\ & & & & 0 & 1 \\ 1 & & & & & 0 \end{pmatrix}, \tag{C5}$$

$$\boldsymbol{M_1} = e^{-g} \begin{pmatrix} 0 & & & & & r_N \\ r_1 & 0 & & & & \\ & r_2 & 0 & & & \\ & & \ddots & \ddots & & \\ & & & r_{N-2} & 0 & \\ & & & & r_{N-1} & 0 \end{pmatrix}. \tag{C6}$$

The zeroth-order eigenvalues and eigenvectors of M_0 are given by

$$\lambda_{k_n}^{(0)} = e^{g+ik_n}, \tag{C7}$$

$$\langle x | \psi_{k_n}^{(0)} \rangle = \frac{1}{\sqrt{N}} e^{ik_n x}, \tag{C8}$$

where

$$k_n := \frac{2\pi n}{N}, \quad n = 0, 1, 2, \cdots, N-1. \tag{C9}$$

By setting

$$\xi_0 = \text{Re}\, \lambda_{k_n}^{(0)} = e^g \cos k, \tag{C10}$$

$$\eta_0 = \text{Im}\, \lambda_{k_n}^{(0)} = e^g \sin k, \tag{C11}$$

we see that the eigenvalues are equidistantly aligned on a circle of radius e^g in the complex λ plane:

$$\xi_0^2 + \eta_0^2 = e^{2g}. \tag{C12}$$

Similarly to Sec. IV, we find the first-order eigenvalue perturbative shift in eigenvalues,

$$\lambda_{k_n}^{(1)} = \langle \psi_{k_n}^{(0)} | A_1 | \psi_{k_n}^{(0)} \rangle = e^{-g-ik_n} \bar{r}(0), \tag{C13}$$

where $\bar{r}(0)$ is the component at $k = 0$ of the Fourier transform of the random variable r_x:

$$\bar{r}(k) = \frac{1}{N} \sum_{x=0}^{N-1} r_{x+1} e^{ikx}. \tag{C14}$$

We can cast it in the following way:

$$\xi_1 := \text{Re}\, \lambda_{k_n}^{(1)} = e^{-g} \bar{r}(0) \cos k_n, \tag{C15}$$

$$\eta_1 := \text{Im}\, \lambda_{k_n}^{(1)} = -e^{-g} \bar{r}(0) \sin k_n, \tag{C16}$$

Note that the first-order perturbation does not depend on the details of the random numbers but only on the average. Since we use the random numbers with a symmetric probability distribution, $\bar{r}(0)$ vanishes in the limit $N \to \infty$. For a finite value of N ($N = 16$), we find the movement of the eigenvalues as illustrated in Fig. 20(a).

The *second*-order eigenvalue perturbation, obtained by similar techniques, is given by

$$\lambda_{k_n}^{(2)} := -\sum_{\substack{m=0 \\ m \neq n}}^{N-1} \frac{\langle \psi_{k_n}^{(0)} | A_1 | \psi_{k_m}^{(0)} \rangle \langle \psi_{k_m}^{(0)} | A_1 | \psi_{k_n}^{(0)} \rangle}{\lambda_{k_m}^{(0)} - \lambda_{k_n}^{(0)}}, \tag{C17}$$

$$= -e^{-3g} \sum_{\substack{m=0 \\ m \neq n}}^{N-1} \frac{e^{-i(k_m+k_n)}}{e^{ik_m} - e^{ik_n}} |\bar{r}(k_n - k_m)|^2, \tag{C18}$$

which we illustrate in Fig. 20(b). The third-order eigenvalue perturbation is illustrated in Fig. 20(c), too. More analyses reveal that the kth-order corrections generally behave as

$$\lambda_k^{(2)} \propto e^{-3g-3ik}, \quad \lambda_k^{(3)} \propto e^{-5g-5ik}. \tag{C19}$$

Although large g perturbation theory is useful for capturing eigenvalue trends, it does not seem capable of determining
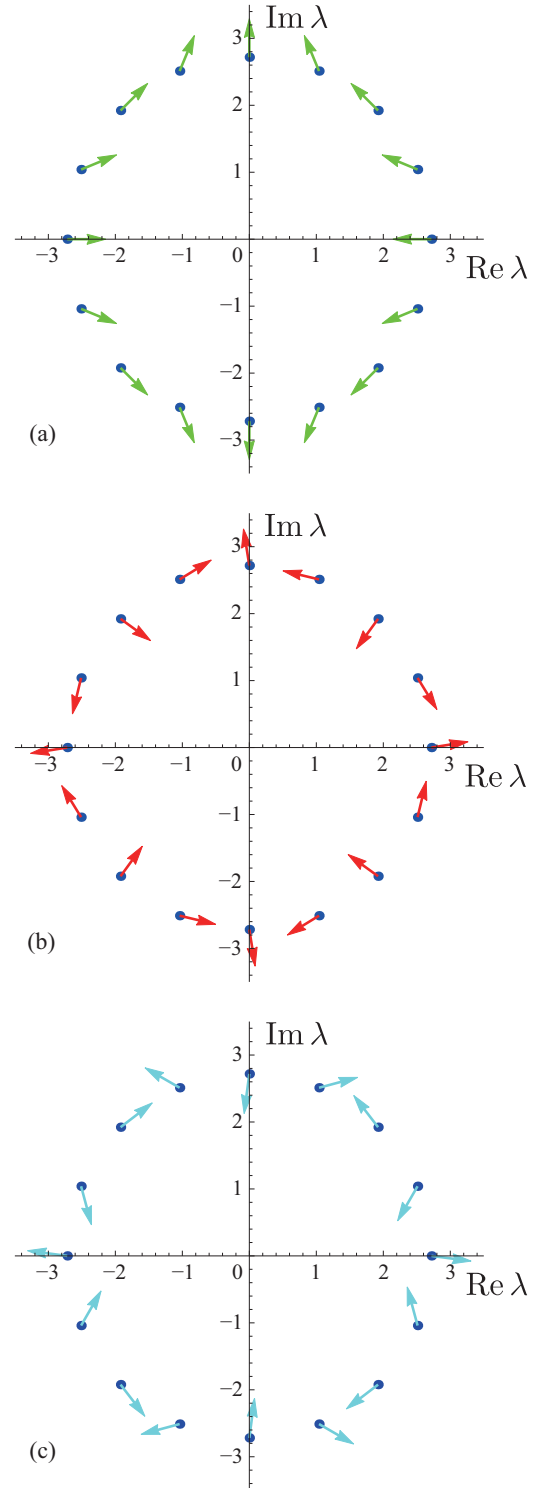

FIG. 20. The directions of eigenvalue perturbations with $N = 16$ and $g = 1$ for a random sample out of a binomial distribution. The blue dots indicate the positions of zeroth-order eigenvalues (C8) in all panels. The arrows in each panel indicate (a) the first-order perturbations (C13) magnified 50 times and (b) the second-order perturbations (C18) magnified 20 times, and (c) the arrows indicate the third-order perturbations magnified 100 times.

when eigenvalues stop moving with increasing g; the corresponding eigenvalues remain delocalized within this approach.

[1] M. L. Mehta, *Random Matrices*, 3rd ed., Vol. 142 (Academic Pressy, New York, 2004).

[2] T. A. Brody, J. Flores, J. B. French, P. A. Mello, A. Pandey, and S. S. Wong, Rev. Mod. Phys. **53**, 385 (1981).

[3] H. J. Sommers, A. Crisanti, H. Sompolinsky, and Y. Stein, Phys. Rev. Lett. **60**, 1895 (1988).

[4] E. P. Wigner, Ann. Math. **62**, 548 (1955); **67**, 325 (1958).

[5] J. Ginibre, J. Math. Phys. **6**, 440 (1965).

[6] V. L. Girko, Teoriya Veroyatnostei I Ee Primeneniya **29**, 669 (1984).

[7] K. Rajan and L. F. Abbott, Phys. Rev. Lett. **97**, 188104 (2006).

[8] P. W. Anderson, Phys. Rev. **109**, 1492 (1958).

[9] B. I. Shklovskii and A. L. Efros, *Electronic Properties of Doped Semiconductors* (Springer-Verlag, Berlin, 1984).

[10] R. Chaudhuri, A. Bernacchia, and X.-J. Wang, Elife **3**, e01239 (2014).

[11] F. L. Metz, I. Neri, and D. Bollé, Phys. Rev. E **84**, 055101 (2011).

[12] I. Neri and F. L. Metz, Phys. Rev. Lett. **109**, 030602 (2012).

[13] H. Rouault, and S. Druckmann, arXiv:1509.01893 (2015).

[14] See, e.g., T. A. L. Ziman, Phys. Rev. Lett. **49**, 337 (1982), and references therein.

[15] D. J. Thouless, J. Phys. C **5**, 77 (1972).

[16] P. Dayan and L. F. Abbott, *Theoretical Neuroscience* (MIT Press, Cambridge, MA, 2001).

[17] J. Hertz, A. Krogh, and R. G. Palmer, *Introduction to the Theory of Neural Computation* (Addison Wesley, Reading, 1991).

[18] O. Shriki, D. Hansel, and H. Sompolinsky, Neur. Comput. **15**, 1809 (2003).

[19] T. P. Vogels, K. Rajan, and L. F. Abbott, Annu. Rev. Neurosci. **28**, 357 (2005).

[20] N. Hatano and D. R. Nelson, Phys. Rev. B **56**, 8651 (1997).

[21] I. Y. Goldsheid and B. A. Khoruzhenko, Phys. Rev. Lett. **80**, 2897 (1998).

[22] D. R. Nelson and N. M. Shnerb, Phys. Rev. E **58**, 1383 (1998).

[23] N. M. Shnerb and D. R. Nelson, Phys. Rev. Lett. **80**, 5172 (1998); see also K. A. Dahmen, D. R. Nelson, and N. M. Shnerb, in *Statistical Mechanics of Biocomplexity* (Springer, Berlin, 1999), pp. 124–151.

[24] K. B. Efetov, Phys. Rev. Lett. **79**, 491 (1997).

[25] P. W. Brouwer, P. G. Silvestrov, and C. W. J. Beenakker, Phys. Rev. B **56**, R4333 (1997).

[26] J. Feinberg and A. Zee, Phys. Rev. E **59**, 6433 (1999).

[27] D. E. Holz, H. Orland, and A. Zee, J. Phys. A: Math. Gen. **36**, 3385 (2003).

[28] S. N. Chandler-Wilde, R. Chonchaiya, and M. Lindner, Operat. Matrices **7**, 739 (2013).

[29] S. N. Chandler-Wilde and E. B. Davies, J. Spect. Theor. **2**, 147 (2012).

[30] S. N. Chandler-Wilde, R. Chonchaiya, and M. Lindner, Operat. Matrices **5**, 633 (2011).

[31] R. Hagger, J. Spect. Theor. **6**, 215 (2016).

[32] R. Hagger, Random Matrices: Theor. Appl. **4**, 1550016 (2015).

[33] B. Derrida, J. L. Jacobsen, and R. Zeitak, J. Stat. Phys. **98**, 31 (2000).

[34] H. Furstenberg, Trans. Am. Math. Soc. **108**, 377 (1963).

[35] K. Ishii, Prog. Theor. Phys. Suppl. **53**, 77 (1973).

[36] A. Crisanti, G. Paladin, and A. Vulpiani, *Products of Random Matrices* (Springer, Berlin, 1993).

[37] L. G. Molinari and G. Lacagnina, J. Phys. A: Math. Theor. **42**, 395204 (2009).

[38] N. Hatano and D. R. Nelson, Phys. Rev. Lett. **77**, 570 (1996).

[39] B. Doiron and A. Litwin-Kumar, Front. Comput. Neurosci. **8**, 56 (2014).

[40] J. D. Seelig and V. Jayaraman, Nature **521**, 186 (2015).

[41] R. M. May, Math. Biosci. **12**, 59 (1971).

[42] R. M. May, Nature **238**, 413 (1972).

[43] M. W. McCoy, B. M. Bolker, K. M. Warkentin, and J. R. Vonesh, Am. Nat. **177**, 752 (2011).

[44] E. Karzbrun, A. M. Tayar, V. Noireaux, and R. H. Bar-Ziv, Science **345**, 829 (2014).

[45] G. Theodorou and M. H. Cohen, Phys. Rev. B **13**, 4597 (1976).

[46] T. P. Eggarter and R. Riedinger, Phys. Rev. B **18**, 569 (1978).

[47] N. Hatano and J. Feinberg, arXiv:1603.06187 (2016).

[48] R. N. Silver and H. Röder, Int. J. Mod. Phys. C **5**, 735 (1994).

[49] R. N. Silver, H. Roeder, A. F. Voter, and J. D. Kress, J. Comp. Phys. **124**, 115 (1996).

[50] R. N. Silver and H. Röder, Phys. Rev. E **56**, 4822 (1997).